Pontifícia Universidade Católica
do Rio de Janeiro

Antonio Weiller Corrêa do Lago

Nonlinear Identification of a Flexible Joint Robotic Actuator Using Proprioceptive and Video Data

Dissertação de Mestrado

Dissertation presented to the Programa de Pós–graduação em Engenharia Mecânica, do Departamento de Engenharia Mecânica of PUC-Rio in partial fulfillment of the requirements for the degree of Mestre em Engenharia Mecânica.

Advisor : Prof. Igor Braga de Paula
Co-advisor: Prof. Helon Vicente Hultmann Ayala

Rio de Janeiro
October 2024

Pontifícia Universidade Católica
do Rio de Janeiro

Antonio Weiller Corrêa do Lago

Nonlinear Identification of a Flexible Joint Robotic Actuator Using Proprioceptive and Video Data

Dissertation presented to the Programa de Pós–graduação em Engenharia Mecânica of PUC-Rio in partial fulfillment of the requirements for the degree of Mestre em Engenharia Mecânica. Approved by the Examination Committee:

Prof. Igor Braga de Paula
Advisor
Pontifícia Universidade Católica do Rio de Janeiro – PUC-Rio

Prof. Helon Vicente Hultmann Ayala
Co-Advisor
Pontifícia Universidade Católica do Paraná - PUC-PR

Prof. Marco Antonio Meggiolaro
Pontifícia Universidade Católica do Rio de Janeiro – PUC-Rio

Prof. Daniel Henrique Braz de Sousa
Instituto Militar de Engenharia - IME

Rio de Janeiro, October the 4th, 2024

Antonio Weiller Corrêa do Lago

Majored in Mechanical Engineering by the Pontifical Catholic University of Rio de Janeiro (PUC-Rio), in 2022.

Bibliographic data

Lago, Antonio Weiller Corrêa do

Nonlinear identification of a flexible joint robotic actuator using proprioceptive and video data / Antonio Weiller Corrêa do Lago ; advisor: Igor Braga de Paula ; co-advisor: Helon Vicente Hultmann Ayala. – 2024.
80 f. : il. color. ; 30 cm

Dissertação (mestrado)–Pontifícia Universidade Católica do Rio de Janeiro, Departamento de Engenharia Mecânica, 2024.
Inclui bibliografia

1. Engenharia Mecânica – Teses. 2. Aprendizagem de máquina. 3. Atuador robótico. 4. Atuador elástico em série. 5. Identificação de sistemas. 6. Visão computacional. I. Paula, Igor Braga de. II. Ayala, Helon Vicente Hultmann. III. Pontifícia Universidade Católica do Rio de Janeiro. Departamento de Engenharia Mecânica. IV. Título.

CDD: 621

Aos meus pais, irmãos e família
pelo apoio e encorajamento.

Acknowledgments

To my parents for their education, attention, and affection at all times, even in the most difficult moments.

To my co-advisor, Prof. Helon Vicente, thank you for the continuous stimulus to improve this work. I am very grateful for his partnership.

To PUC-Rio and the Department of Mechanical Engineering for all administrative and technical support.

This study was financed in part by the Coordenação de Aperfeiçoamento de Pessoal de Nível Superior - Brasil (CAPES) - Finance Code 001

Abstract

Lago, Antonio Weiller Corrêa do; Paula, Igor Braga de (Advisor); Ayala, Helon Vicente Hultmann (Co-Advisor). **Nonlinear Identification of a Flexible Joint Robotic Actuator Using Proprioceptive and Video Data**. Rio de Janeiro, 2024. 80p. – Departament of Mechanical Engineering, Pontifical Catholic University of Rio de Janeiro.

In the context of human interactive robotics, there is a growing interest in Series Elastic Actuators (SEA), driven by the critical need to ensure safety and functionality. Moreover, a precise model is required to obtain optimal control. However, the inherent nonlinearities of those actuators, such as friction, gear backlash, and noise, greatly increase the challenge of controlling and modeling such devices. Furthermore, a compliant element adds a new nonlinearity, making the modeling task more challenging. Aiming to tackle these issues, this work proposes extensive system identification to obtain mathematical models characterizing the dynamics of an original low-cost elastomer-based SEA. The proposed methodologies investigate different characteristics of the system. The first focuses on modeling the elastic joint's nonlinearities through a hybrid model. The second contribution aims to examine the accuracy of physics-informed neural networks for gray-box identification of friction parameters. Lastly, a framework to obtain the states of the assembly using video is proposed. From these estimations, a gray-box identification using video is proposed. All three studies use the data from the actuator assembly. The first two contributions obtained important results indicating the efficiency of the proposed methodologies. The third contribution showed the potential of the novel video-based identification approach.

Keywords

Computer Vision; Machine Learning; Robotic actuator; Series Elastic Actuator; System Identification.

Resumo

Lago, Antonio Weiller Corrêa do; Paula, Igor Braga de; Ayala, Helon Vicente Hultmann. **Identificação Não Linear de um Atuador Robótico com Junta Flexível Usando Dados Proprioceptivos e de Vídeo**. Rio de Janeiro, 2024. 80p. Dissertação de Mestrado – Departamento de Engenharia Mecânica, Pontifícia Universidade Católica do Rio de Janeiro.

No contexto de robos colaborativos, há um crescente interesse em Atuadores Elásticos em Série impulsionado pela necessidade de garantir segurança e funcionalidade. No entanto, as não linearidades inerentes a esses atuadores, como atrito, folga nas engrenagens e ruído, aumentam significativamente o desafio de controlar e modelar tais dispositivos. Além disso, um elemento elástico adiciona uma nova não linearidade. Visando essas características, este trabalho propõe um extenso trabalho de identificação do sistema para obter um modelo para um atuador elástico em série baseado em elastômero de baixo custo e original. As metodologias propostas investigam diferentes características do sistema. A primeira se concentra em modelar as não linearidades da junta elástica por meio de um modelo híbrido. A segunda contribuição visa examinar a precisão de redes neurais informadas por física para identificação de caixa cinza de parâmetros de atrito. Por último, é proposto uma metodologia para obter os estados da montagem usando vídeo. A partir dessas estimativas, é proposta uma identificação de caixa cinza usando vídeo. Todos os três estudos utilizam os dados da montagem do atuador. As duas primeiras contribuições obtiveram resultados importantes indicando a eficiência das metodologias propostas. A terceira contribuição mostrou o potencial da nova abordagem de identificação baseada em vídeo.

Palavras-chave

Aprendizagem de Máquina,; Atuador robótico; Atuador Elástico em Série; Identificação de Sistema; Visão Computacional.

Table of Contents

List of Figures

List of Tables

List of Abreviations

AI – Artificial Intelligence

ANN – Artificial Neural Network

ML – Machine Learning

COBOTS – Collaborative Robots

DT – Digital twin

CNN – Convolutional Neural Network

SEA – Series elastic actuator

NARX – Nonlinear Autoregressive with Exogenous Input

ARMAX – AutoRegressive Moving Average with Exogenous Inputs

ARX – AutoRegressive Exogenous Inputs

LVSA – Lightweight Variable Stiffness Actuator

VAF – Variance-accounted-for

PINNs – Physics-informed neural networks

PDE – Partial differential equations

ODE – Ordinary differential equations

LSTM – Long short-term memory

OSA – One Step Ahead

FR – Free Run

DNN – Deep Neural Network

RMSE – Root Mean Squared Error

MAE – Mean Absolute Error

NRMSE – Normalized Root Mean Squared Error

FIT – Fit Percentage

eSEA – elastomer-based SEA

DNN – Deep Neural Networks TL – Transfer Learning

GPU – Graphics Processing Units

TPU – Tensor Processing Units

ReLu – Rectified Linear Unit‘

FLOPS – Floating Point Operations Per Second

PGNN – Physics-Guided Neural Networks

Un exemple n'est pas forcément un exemple à suivre

Albert Camus, *Le Mythe de Sisyphe.*

1
Contextualization

Artificial Intelligence (AI) has witnessed a meteoric rise in the past decade, permeating various facets of human life and transforming industries worldwide [1]. Stanford Professor John McCarthy defined AI in 1955 as "the science and engineering of making intelligent machines" [2]. Although the algorithms have become more effective over the past years, the main foundations of AI are based on the human brain and human reasoning [3]. Artificial neural networks (ANN) are based on the human brain, more specifically on the neurons and their interconnections [4, 5]. Biological algorithms have seen incredible success because of multiple factors, from the rise of data availability to the improvement in computing performance and the development of new architectures [6, 7].

Machine learning (ML) is one of the main branches of AI, learning complex tasks from data [8]. Consequently, ML applications are spreading across a broad spectrum of domains, including medicine and healthcare [9–12] as well as cybersecurity [13–15]. One of the main tasks of ML is obtaining a model capable of discovering mathematical relationships within data [16]. This technique allows us to model highly complex and nonlinear phenomenons [17].

One of the fields that has seen a rise in ML solutions has been robotics [18]. Allowing the robots to become more intelligent, efficient, and adaptable to complex tasks, such as autonomous navigation, object recognition and manipulation, natural language processing, and predictive maintenance [18–20]. With the development of Industry 4.0, one type of robot that has seen an emergence has been collaborative robots (COBOTS) [21]. These types of robots aim to assist the human worker instead of replacing them with lower speeds and higher safety concerns [22, 23]. Barclays research report indicates the market share of COBOTS is expected to grow from 116 million US dollars in 2015 to 11.5 billion US dollars in 2025, with sales surpassing 700,000 units a year in 2025 [23]. These have significantly improved the efficiency, agility, and resilience of many industries, including medicine, logistics, warehousing, farming, and manufacturing [23–28].

Accompanying the wave of AI, concepts such as Digital Twin (DT) have seen an exponential growth with the advent of Industry 4.0 [29]. In [30] Glaessgen and Stargel defined a DT as a multi-physics, multi-scale and probabilistic simulation of a complex system that uses the best available physical models, sensor updates, and so on to simulate the life of its corresponding twin. ages

of having DTs are extensive, in general, these can replace wasted physical resources, by replacing the physical test saving time, energy, or material and costs. These DT can be applied in multiple industries including fields such as medical, industrial, aerospace, robotics and climate change [31].

The construction of a DT can be a challenging task. In order to obtain DT models capable of real-time simulations with the role of replicating a real life complex system, a highly accurate, reliable and interpretable model is required. Depending on the application, the models can be simple but in the engineering fields these can have a high complexity and a high number of variables [32]. Two main approaches have been proposed to obtain precise dynamic model, physics-based modeling and system identification, which includes data-driven models. The aim of system identification is to obtain a mathematical model from input-output data of a system. Physics-based modeling has been the backbone in most engineering applications and relied on physical observations of processes and materials to obtain dynamic models [33]. With the growing complexity of systems and need for highly precise models in some industries, these physical models are not enough. One example of systems with complex dynamics and a high number of states are COBOTS.

One of the most common methods to augment COBOTS safety is using series elastic actuator (SEA) designs [34]. These consist of using a spring in series with a stiff actuator [35]. Adding joint compliance provides advantages such as shock tolerance, high-fidelity force control, passive energy storage, lower reflected inertia, and higher tolerance to impact loads [36–38]. Notwithstanding the benefits mentioned above, the compliant actuators introduce additional challenges, more specifically, a motion control problem [39]. To realize the full potential of SEAs in advanced robotics, their position and force control capabilities need to be refined [40]. A possible solution is to use a model-based controller [41]. In order to optimize the performance of the model-based controller, not only a highly accurate model is necessary, but also an efficient one to meet real-time requirements [42, 43]. Modeling robots is already challenging due to the multiple nonlinearities and complex phenomena involved [35]. By adding a soft element, new issues arise in modeling and control due to the complex behaviors added from the nonlinearity and hysteresis [28].

One of the ways to obtain accurate models to describe nonlinear phenomena is by using system identification, a technique to find precise representations with varying quantities of information about the system [44].

2
Literature Review and Contributions

System identification has seen a rise in popularity thanks to data availability and improvements in ML algorithms and computing capacities [45]. The choice of identification technique depends on the quantity and quality of available data and the level of prior knowledge about the system [46]. Two main approaches exist within the field of system identification, other than the white-box methodology that relies solely on physical observation. The black-box methodology relies solely on data to obtain a model describing the system [47]. The second approach is a hybrid between the black-box and white-box modeling, called gray-box modeling. The approach relies on both physical and data to obtain a precise model representing the dynamics of a system.

The black-box approach has seen significant growth in many fields due to its easy implementation and low computational cost [48]. Multiple algorithms have been proposed over the years. Within the context of robotics, [49] proposed a model-based controller for 3-DoF Delta Parallel Robot using two models obtained through black-box identification. The first model employed an AutoRegressive Moving Average with Exogenous Inputs (ARMAX) model, and the second used the Nonlinear AutoRegressive with Exogenous input (NARX) methodology with an ANN as the nonlinear algorithm. Both model-based controllers outperformed classical controllers, with the NARX-ANN model yielding the most favorable results with a significant decrease in Root Mean Squared Error (RMSE) errors. Wang *et al.* [50] developed a lightweight variable stiffness actuator (LVSA) using a novel mechanism. Following the design, in order to obtain the most accurate model, the parameters of the actuator are identified, obtaining precise results with a variance-accounted-for (VAF) factor of 88.67%.

Although the black-box model shows outstanding results with limited information, an important downside of algorithms such as ANN is the interpretability aspect. Application fields, such as medicine, criminal justice, and finance, require interpretable models [51]. In engineering fields such as structural engineering, civil engineering, and mechanical engineering, interpretable models are also required [52–54]. So, gray-box modeling is used to obtain greater accuracy while maintaining interpretability by estimating parameters of physics-based models [55].

Physics-informed neural networks (PINNs) were introduced in [56] and can be used to solve partial differential equations (PDE) problems with a data-

driven solution. This was done by adding underlying physical laws as prior information to the deep neural networks, adding constraints such as equations, initial, and boundary conditions in the loss function when optimizing the parameters of the network [57, 58]. This innovative algorithm has shown promising results in parameter identification. Daneker *et al.* [59] showed the adequate performance of the PINNs to identify the unknown parameters of an ODE representing the ultridian endocrine model for glucose-insulin interaction.

In recent years, new algorithms have been developed capable of processing high-dimensional data such as images, sound, and video. The main algorithms include deep Convolutional Neural Networks (CNNs) and Transformers. Deep CNNs can classify images from the ImageNet database [60] with 90% accuracy [61]. Transformers employ a self-attention mechanism and enable parallel processing to achieve remarkable results in Natural Language Processing (NLP) tasks [62]. These algorithms have contributed significantly to the field of system identification and the use of video for state observation and identification purposes. [63] implemented a deep auto-encoder using video to estimate the position of a ball from the video frames and make future predictions using the state estimates from the encoder. Although the system can be considered simple, the results show the methodology's potential.

Jaques *et al.* [64] proposed an unsupervised vision-based identification approach, without using neural networks, composed of three steps to make the parameter estimation. The first steps involve extracting the system's key points from the video, transforming them to the world coordinates, and optimizing the system's physical parameters and initial conditions. Lastly, the most likely trajectory is predicted. The unsupervised methodology shows a good overall performance in obtaining the key points and tracking both a bouncing ball and a robotic arm without requiring measurements. However, the parameter estimation is only done for the bouncing ball, a system that can be considered relatively simple. In the context of robotics, contributions using video data include advances in state estimation [65, 66], calibration framework for robotic manipulators [67], and inferring accurately dynamics from video [68]. Although these works have shown positive results in their respective fields, the lack of interpretability often associated with these black-box methodologies is an important downside. Given that context, the emergence of vision-based parameter estimation methods has shown impressive results by combining both neural networks and dynamics constraints [69]. Hofherr *et al.* [70] proposes to make the parameter estimation from a single video combining neural implicit representation with neural ordinary differential equations (ODEs). Additionally, the methodology allows for the rendering of images with selected param-

eters. The performance obtained shows the high potential of the identification technique. However, the examples shown rely on relatively simple systems with few nonlinearities.

2.1 Objectives

The general objective of this work is the application of novel identification methodologies to model the dynamics of an eSEA assembly. The work is composed of three case studies with the following specific objectives.

1. To propose a hybrid model using a linear and a nonlinear algorithm to characterize the dynamics of an elastic joint from an original elastomer-based SEA;

2. To propose an efficient machine learning model to perform the gray-box identification of the dynamics of an eSEA assembly. More specifically, to optimize the parameters of multiple friction models;

3. To develop a deep learning-based framework for the gray-box identification of a single series elastic robot actuator from video.

The three case studies use data obtained experimentally from an original elastomer-based SEA assembly developed by [71].

2.2 Contributions

In the following, the contributions of this thesis are established and divided into three items:

– Identification of an Elastic Joint of an Elastomer-based Series Elastic Actuator (presented in Chapter 7)

  * Propose and compare a novel nonlinear hybrid model of a flexible joint of an original low-cost elastomer-based SEA ;
  * Validate the method by comparing it to other nonlinear algorithms.

  This chapter has been published as a conference paper:

  LAGO, A. W. C. ; CAMERINI, I. G. ; SOUSA, L. C. ; SOUSA, D. H. B. ; LOPES, F. R. ; MEGGIOLARO, M. A. ; AYALA, H. V. H.. **Black-Box Identification with Static Neural Networks of Nonlinearities of an Elastomer-Based Elastic Joint Manipulator**. In: 2023 INTERNATIONAL JOINT CONFERENCE ON NEURAL NETWORKS. Queensland, Australia, 2023. IEEE.

– Physics-informed and black-box identification of a robotic actuator with a flexible joint (presented in Chapter 8)

    * Propose a methodology of PINNs for the gray-box identification of an original low-cost elastomer-based SEA ;
    * Validate the method by identifying the parameters of various friction models and comparing them to other ML algorithms.

  This chapter has been published as a conference paper:

– LAGO, A. W. C.; SOUSA, DE SOUSA, D. H. B.; HENRIQUE DOMINGUES, P.; DANEKER, M.; LU, L. ; AYALA, H. V. H.. **Physics-informed and black-box identification of a robotic actuator with a flexible joint**. 20th IFAC Symposium on System Identification. Boston, USA, 07 2024.

– Identification of the friction model of an elastomer-based SEA from video (presented in Chapter 8)

    * Propose a novel framework to perform the gray-box identification of an actuator from video ;
    * Compare the model measurements and the simulation estimation using the identified parameters to the experimental data.

  This chapter has been published as a conference paper:

– LAGO, A. W. C.; SOUSA, DE SOUSA, D. H. B.; LU, L. ; AYALA, H. V. H.. **Identification of the friction model of a single elastic robot actuator from video**. 20th IFAC Symposium on System Identification. Boston, USA, 07 2024.

Additionally, the following papers have been published in conference proceedings and journals as a result of collaboration throughout the completion of the present thesis:

– SOUSA, D. H. B.; LOPES, F. L.; LAGO, A. W. C.; MEGGIOLARO, M. A.; AYALA, H. V. H. **Hybrid Grey and Black-box Nonlinear System Identification of an Elastomer Joint Flexible Robotic Manipulator**. *Mechanical Systems and Signal Processing*, 200:110405, 2023.

– LAGO, A. W. C. ; SOUSA, L. C. ; SOUSA, D. H. B. ; LOPES, F. R. ; MEGGIOLARO, M. A. ; AYALA, H. V. H.. **Identificação usando método não linear de um sistema de posicionamento**. In: 2022 XXIV CONGRESSO BRASILEIRO DE AUTOMÁTICA. Fortaleza, Brazil, 2022. SBA.

– LAGO, A. W. C.; SOUSA, L. C.; DE SOUSA, D. H. B.; LU, L. ; AYALA, H. V. H.. **Pose estimation of robotic manipulators using deep transfer learning towards video-based system identification**. Simpósio Brasileiro de Automação Inteligente (SBAI 2023). Manaus, Brazil, 10 2023. SBA.

– FERNANDES, D. L.; LOPES, F. R.; DO LAGO, A. W.; DE SOUSA, D. H. B.; MEGGIOLARO, M. A. ; AYALA, H. V. H.. **System identification of an elastomeric series elastic actuator using black-box models**. 2023 31st Mediterranean Conference on Control and Automation (MED). Limassol, Cyprus, p. 569–574. IEEE, 2023.

2.3 Organization

This work is divided into four main parts. Part 1 focuses on introducing the thesis and giving the proper context through the literature review and, lastly, providing the motivation, objectives, and contributions of the work.

Part II defines the concepts used in this work. Section 3 presents the theoretical basis of system identification, which involves determining the methodologies adopted, the fundamental concepts, and the validation metrics. Following that, Section 4 defines the mathematical concepts behind the neural network architectures used in the case study. Lastly, Chapter 5 briefly describes the existing friction models and their respective equations.

Part III describes the experimental system used in all three contributions and presents the mathematical equations characterizing the system. Initially describing the different components of the assembly. Following that, the mathematical modeling is defined. Finally, the data acquisition steps and parameters are described.

Part IV presents this thesis's fundamental contributions. The first study focuses on obtaining a mathematical representation of the elastic joint dynamics. The second case study is devoted to comparing and testing the performance of the PINNs model for gray-box identification purposes, optimizing the friction parameters of the system. Lastly, the last contribution proposes a framework to identify friction parameters from the eSEA assembly using states obtained using video.

Finally, the final remarks are presented in Part V, through a conclusion and respective future works suggestions.

Part II

Background Review

3
System Identification

The main focus of this thesis is system identification. System identification has seen a soar in popularity in the past years for multiple reasons, from improvements in ML and AI algorithms to improvements in computers and access to data[72]. These improvements and the need for precise mathematical models describing complex systems have made system identification a vital tool and topic in multiple industries. The system identification methodology has been defined previously [73] and can be described by Figure 3.1.

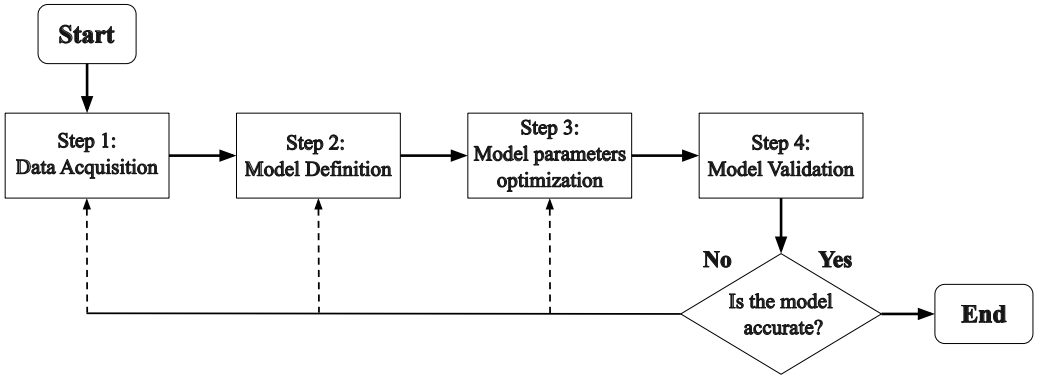

Figure 3.1: System identification procedure.

One of the main decisions that must be made is the type of identification you want. The first, the analytical model, or white-box modeling, relies on a purely physical interpretation to describe the phenomena mathematically. The gray-box modeling relies on physical insights and data to estimate some parameters of a predefined model [74]. Lastly, the black-box approach relies purely on data to find a suitable model structure to describe the different nonlinearities.

This chapter defines the different algorithms used for the various works presented in this thesis. The first sections focus on exploring gray-box and black-box methodologies. Firstly, the linear and nonlinear black-box models, ARMAX and NARX, respectively. Following that, the PINNs model is presented. Moreover, it presents novel training methods and validation metrics.

3.1
System Identification

This section focuses on presenting different identification methods and algorithms. There are two black-box models: a linear model with the ARMAX

model and the NARX-ANN model as the nonlinear model. Following that, a gray-box model is presented in the PINNS, employing neural networks to automatically differentiate and optimize the parameters of an ODE.

3.1.1 ARMAX

The Autoregressive Moving Average with Exogenous Input Model (ARMAX) is a linear parametric identification technique [73]. Through the use of past inputs and outputs, the algorithm estimates the future states of the system. The general ARMAX model is given by

$$A(z^{-1})y(k) = \frac{B(z^{-1})}{F(z^{-1})}u(k) + \frac{C(z^{-1})}{D(z^{-1})}\xi(k) \tag{3-1}$$

where $u(k)$, $y(k)$ are the system input and output, $\xi(k)$ is a noise sequence. And $A(z^{-1})$, $B(z^{-1})$, $C(z^{-1})$, $D(z^{-1})$, and $F(z^{-1})$ are the polynomials concerning the backward shift operator, which are defined by

$$A(z^{-1}) = 1 + a_1 z^{-1} + ... + a_{n_a} z^{-n_a} \tag{3-2}$$

$$B(z^{-1}) = 1 + b_1 z^{-1} + ... + b_{n_b} z^{-n_b} \tag{3-3}$$

$$C(z^{-1}) = 1 + c_1 z^{-1} + ... + c_{n_c} z^{-n_c} \tag{3-4}$$

$$D(z^{-1}) = 1 + d_1 z^{-1} + ... + d_{n_d} z^{-n_d} \tag{3-5}$$

$$F(z^{-1}) = 1 + f_1 z^{-1} + ... + f_{n_f} z^{-n_f} \tag{3-6}$$

where n_a, n_b, n_c, n_d, and n_f are the orders of the model.

3.1.2 NARX

The Nonlinear autoregressive exogenous model (NARX) is a technique that uses a nonlinear algorithm that uses the system's past inputs and outputs to make future state predictions[75]. The mathematical representation can be given by

$$\hat{y}(k) = F[y(k-1), ..., \ y(k-n_y), u(k), u(k-1), ..., u(k-n_y)] + \eta(k) \tag{3-7}$$

where $u(k)$, $y(k)$, and $\eta(k)$ are the input, output, and noise sequences, respectively, and n_y and n_u are the delays related to output and input. In the NARX model, the function F is commonly represented by a nonlinear function from a polynomial to a neural network. The nonlinear function optimized in

the NARX model is the multi-layer artificial neural network depicted in Figure 3.2.

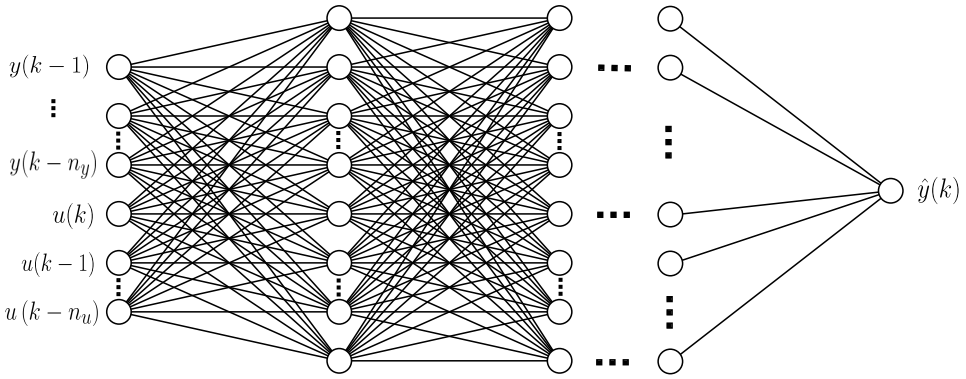

Figure 3.2: NARX-ANN schematic.

3.2 Physics-informed Neural Networks

In [56], Raissi *et al.* developed physics-informed neural networks with the objective of facilitating neural network training by adding laws of physics describing the system as constraints. This allowed initially for two types of applications: a data-driven solution of partial differential equations (PDEs) and a data-driven discovery of PDEs. Considering ODEs are simplified PDEs, with only one independent variable, PINNs can easily be implemented for ODEs problems. This thesis focuses on the second application, which allows for using PINNs for gray-box problems.

The first element composing PINNs is the deep neural network (DNN), represented on the left of Figure 3.3. The DNN is similar to the neural network in Section 3.1.2. The only difference is that it does not necessarily use multiple past states and excitation signals; it relies mainly on time as a variable and other known states and excitation inputs depending on the

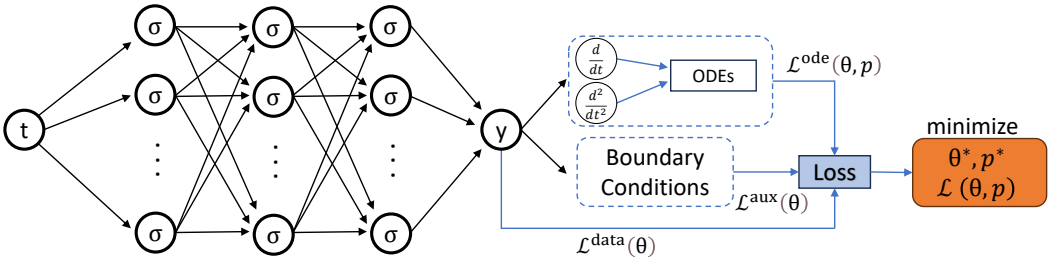

Figure 3.3: PINNs diagram.

system. The network weights and biases are optimized to model the system's nonlinearities, obtaining the outputs from the inputs.

Another important concept PINNs utilize is automatic differentiation. If time (t) is the input, they use the input coordinates and model parameters to differentiate the outputs, obtaining the derivatives of the states [76]. Where the forward pass computes the values of the variables and the backward pass the derivatives, only one pass is required, making it highly efficient compared to other methods.

The following step is to optimize the loss function, which is composed of physical laws, initial conditions, boundary conditions, and measured observation. The ODEs describing the system dynamics are solved, and the system's parameters are optimized to minimize the loss [77].

The training of PINNs is usually done through multiple steps. The first step is to train the DNN, given the measured observations about the system. After this initial training, the DNN's weights and biases may be frozen to optimize the ODE's parameters, depending on the objective [78]. In the third contribution, the objective is to perform a gray-box identification of friction parameters; with that in mind, the technique cited above is used.

3.3 Prediction types

Two main prediction types exist after defining the amount of previous input and output used to make future predictions [79]. The first, *One Step Ahead* (OSA) prediction makes estimations of the next state of the system using previous input and measured outputs [80]. The *Free Run* (FR) prediction type only relies on an initialization with measured output to initialize the model. The predictions are made using previous input and previously predicted outputs obtained using the model.

The prediction model that performs well during free run simulation shows a more robust performance. The error is propagated from the previous model prediction, considering the last output model becomes the input for the following estimation.

3.4 Validation metrics

This section defines the validation metrics used in this thesis. Validation metrics play an important role in understanding the results and evaluating the performance of the models [81].

The metrics used are the Root Mean Squared Error (*RMSE*, the Mean Absolute Error (MAE), the determinant coefficient evaluates the performance of the model given by R^2, the Variance Accounted-For (VAF) for the correlation analysis, the Normalized Root Mean Squared Error expressed as a percentage, called the Fit Percent (FIT). Their respective mathematical representation are

$$RMSE = \sqrt{\frac{1}{n}\sum_{j=1}^{n}\left(y_j - \hat{y}_j\right)^2} \tag{3-8}$$

$$MAE = \frac{1}{n}\sum_{j=1}^{n}\left|y_j - \hat{y}_j\right| \tag{3-9}$$

$$R^2 = \frac{\sum_{j=1}^{n}\left(y_j - \hat{y}_j\right)^2}{\sum_{j=1}^{n}\left(y_j - \bar{y}_j\right)^2} \tag{3-10}$$

$$VAF = 100\left(1 - \frac{var(y_j - \hat{y}_j)}{var(y_j)}\right) \tag{3-11}$$

$$FIT = 100\left(1 - \frac{\sum_{j=1}^{n}\left|y_j - \hat{y}_j\right|}{\sum_{j=1}^{n}\left|y_j - \bar{y}_j\right|}\right) \tag{3-12}$$

considering y_j as the measured data, $\hat{y}_j$ as the simulated data and $\bar{y}_j$ as the mean value of the measured data.

4
Neural networks

This chapter introduces different neural network architectures used in the contribution, mainly in the third contribution, presented in Chapter 9. The first architecture is the LSTM model, secondly the CNN and the transfer learning methodology.

4.1
Long Short-Term Memory

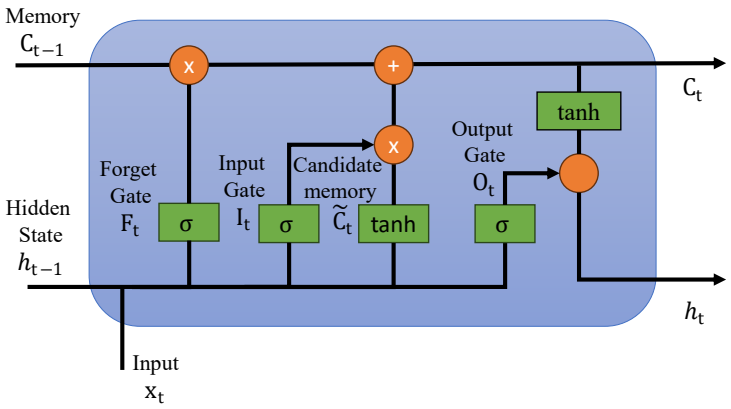

Figure 4.1: LSTM schematic.

Long Short-Term Memory (LSTM) networks are neural networks designed to effectively capture temporal patterns within sequential data [82]. The components of an LSTM cell, presented in Figure 4.1 include a cell state (C_t), an input gate (i_t), a forget gate (F_t), an output gate (o_t), and a hidden state (h_t). The cell state, representing the long-term memory, is updated through the following equations

$$F_t = \sigma(W_f \cdot [h_{t-1}, x_t] + b_f) \tag{4-1}$$

$$i_t = \sigma(W_i \cdot [h_{t-1}, x_t] + b_i) \tag{4-2}$$

$$\tilde{C}_t = \tanh(W_c \cdot [h_{t-1}, x_t] + b_c) \tag{4-3}$$

$$C_t = F_t \cdot C_{t-1} + i_t \cdot \tilde{C}_t \tag{4-4}$$

$$o_t = \sigma(W_o \cdot [h_{t-1}, x_t] + b_o) \tag{4-5}$$

$$h_t = o_t \cdot \tanh(C_t) \tag{4-6}$$

where x_t represents the input at time t, W_f, W_i, W_c, and W_o are weight matrices; b_f, b_i, b_c, and b_o are bias vectors; σ denotes the sigmoid activation function, and tanh is the hyperbolic tangent activation function [83]. The forget gate f_t, input gate i_t, and output gate o_t control the flow of information into and out of the cell state, allowing LSTMs to capture and retain relevant information over extended sequences effectively [84].

4.2 Convolutional Neural Networks

CNNs are designed to process data with multidimensional arrays, accepting 2D and 3D inputs such as color or gray image data compared to other neural networks [85].

The first layers of CNNs are the convolution and pooling layers composing the feature extraction section of the architecture, as can be seen in Figure 4.2. The first layer performs the convolution operation using feature maps. The feature maps, or kernels, slide throughout the image and extract the features from an image [86].

Following these operations, the feature maps obtained through the convolution operations are passed through a non-linear function, for example, ReLU. The pooling layer reduces the resolution of the feature map without losing the critical features. The most common pooling techniques are max pooling, which provides the biggest value from a subregion, and average pooling, which calculates the average from a subregion of the array. The repetition of these two layers composes the feature extraction layers. Other layers, such as batch normalization layer and dropout layers, can be added depending on the task and architecture chosen.

Following the feature extraction layers, the feature maps are flattened and fed into a fully connected neural network to perform the regression or classification task.

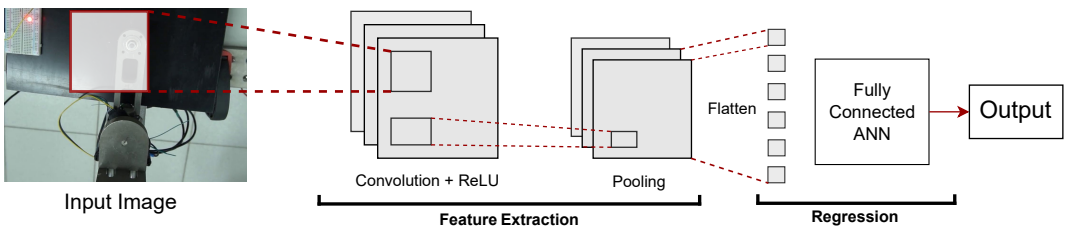

Figure 4.2: CNN schematic.

4.3 Transfer Learning

The complexity and size of deep learning models have increased exponentially in the past years. The improvements in GPUs and TPUs have allowed larger and more complex deep-learning models to be trained [87]. As mentioned in the previous section, CNN models can be separated into two parts: feature extraction and regression or classification layers, depending on the task at hand. With this idea in mind, Transfer Learning (TL) allows the training of deep learning models using a fraction of the time, data, and computational cost while obtaining excellent performances [88].

The technique uses deep CNNs that have already been fine-tuned and trained on large labeled datasets to extract image features and utilizes these trained weights and biases for a new task. Instead of training the whole model, only the last layers are trained for the new task, considering the first layers are feature-extracting and are polyvalent for multiple problems. This is done by freezing the weights and biases of the initial layers and only training the last layers for the new task, lowering the number of parameters that must be trained and reducing the computational cost considerably.

In the context of this work, this technique is used in the third contribution, presented in Chapter 9, more specifically in the context of processing video frames and obtaining mathematical insights on the dynamics of the model.

5
Friction Models

The second and third contributions aim to obtain the parameters of friction models to represent the dynamics of the eSEA. In fact, friction has been studied extensively, and multiple models have been proposed to characterize the highly nonlinear phenomena involved [89]. Friction plays an important role in mechanical systems and is inherent to most systems that have contacting surfaces with relative motion [90, 91].

Friction models can be divided into two types: static friction models and dynamic friction models.

One of the simplest models is the viscous friction model, which only considers the viscous friction force, representing a linear relationship between the relative velocity and the constant friction force. The equation describing the viscous friction model is given by

$$F_f = f_v \dot{\delta} \tag{5-1}$$

where $\dot{\delta}$ is the velocity, and f_v the viscous friction coefficient.

One of the first models was proposed by Coulomb in [92], based on the principle that friction opposes relative motion. Throughout the years, the initial model was improved in order to consider more phenomena, such as the Stribeck effect [93]. This ensures that the decrease from static to kinetic friction is continuous, in other words, the friction force diminishes when the relative motion increases [93, 94]. With that, the Coulomb-Stribeck model takes into account more friction elements. The effect is given by

$$g(v) = f_c + (f_s - f_c) e^{(\dot{\delta}/\dot{\delta}_{Stribeck})^2} \tag{5-2}$$

where the Coulomb coefficient is f_c, the static friction coefficient is f_s and the Stribeck velocity is $\dot{\delta}_{Stribeck}$. Given that, the Coulomb-Stribeck friction model is:

$$F_f = f_v \dot{\delta} + \left[f_c + (f_s - f_c) e^{(\dot{\delta}/\dot{\delta}_{Stribeck})^2} \right] sign(\dot{\delta}) \tag{5-3}$$

The static friction approaches are limited in capturing more complex friction phenomena, such as pre-sliding displacement and frictional lag. The following models are "dynamic" friction models.

The Dahl friction model was developed in 1968 with the aim of representing the friction behavior of ball bearings [95]. By analyzing the stress-strain curve of materials, Dahl observed that the friction force is dependent on relative velocity and displacement. Deriving the stress-strain curve differential equation with time and introducing a new state, z, which represents the displacement in the pre-sliding stage (see [90] for the detailed description of the bristles and its equations).

Through this representation, the Dahl model adds a delay to the original Coulomb model, a memory effect, allowing it to capture the transient behavior of friction [95, 96]. The following equation describes the model

$$F_f = \sigma_0 z \tag{5-4}$$

$$\frac{dz}{dt} = \dot{\delta}\left(1 - \frac{\sigma_0 z}{f_c} sgn(\dot{\delta})\right) \tag{5-5}$$

where σ_0 is the rigidity coefficient.

The last model is the LuGre friction model proposed in [97], deriving the Dahl model and the other models defined previously [98]. This model captures the Stribeck and Stiction effects while considering the bristle deflection. The bristle effect models the spring-like behavior of the surface during the Sticking phase [90]. With this model, it is possible to capture the following friction effects: stiction, stick-slip, Stribeck, Hysteresis, and zero slip displacement.

With the Stribeck velocity-dependent function $g(\dot{\delta})$ instead of a constant, an additional damping σ_1 is associated with micro-displacement [99]. The two following equations represent the LuGre model

$$F_f = \sigma_0 z + \sigma_1 \frac{dz}{dt} + \sigma_2 \dot{\delta} \tag{5-6}$$

$$\frac{dz}{dt} = \dot{\delta}\left(1 - \frac{\sigma_0 z}{g(\dot{\delta})} sgn(\dot{\delta})\right) \tag{5-7}$$

where σ_2 is the viscous friction. These models are used in two of the contributions, with the objective of characterizing the joint friction of a robotic manipulator described in the following part.

Part III

Experimental System

6
Case Study

This chapter focuses on the thesis's primary case study. The assembly is presented through diagrams and pictures showing the different components. The robotic actuator dynamic system is then described mathematically using the different friction models for the identification task.

The assembly is an eSEA assembly developed and described by Felipe Lopes in [71]. Figure 6.1 shows the assembly through pictures and schematics.

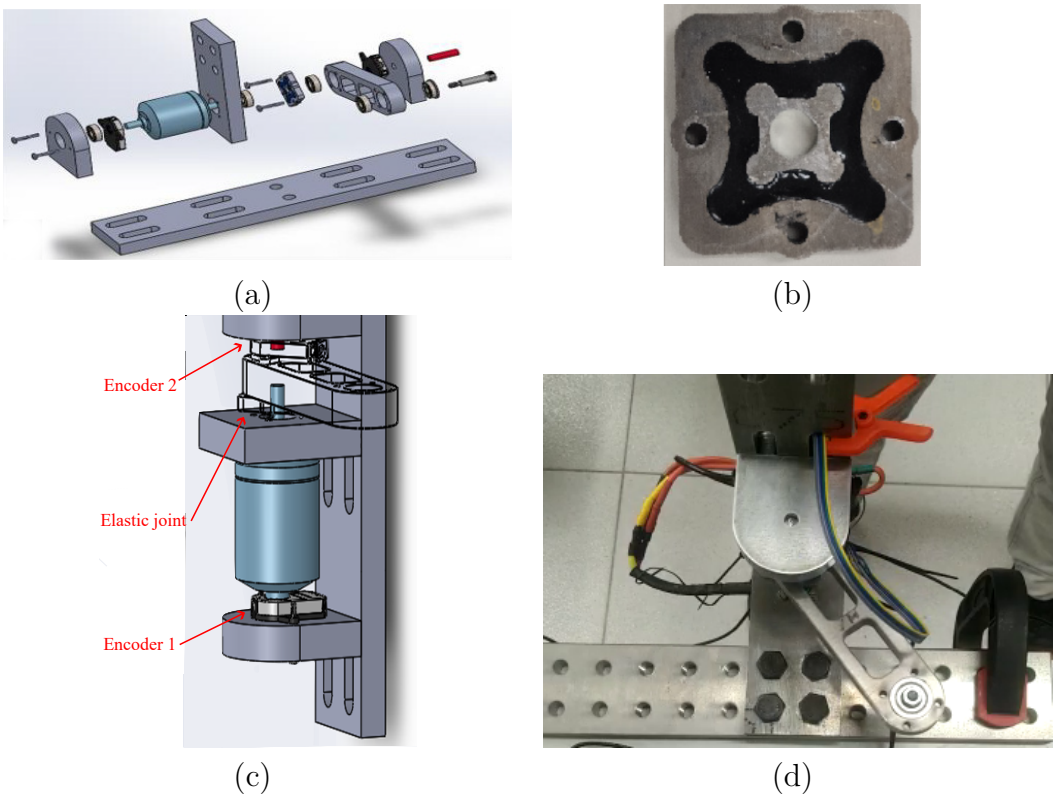

(a) (b) (c) (d)

Figure 6.1: (a) Assembly exploded view. (b) Elastometer-based elastic joint 55A. (c) Assembly detail. (d) Assembled eSEA.

Figure 6.1a shows the exploded view of the assembly, showing the different components of the system. The manipulator base structure and link are built from 7075-T6 aluminum. The assembly's dual shaft D5065/270KV brushless DC motor has a maximum torque of 1.99 Nm.The assembly is powered by a Gophert CPS-6005 power supply and controlled via an open-source Odrive Robotic board. The motor shaft and the link are joined by an elastic joint composed of a 55 Shore-A compliant element (rubber) shown in Figure 6.1b. The angular measurements of the motor shaft and the link are

measured using two CUI AMT 102 encoders with 8192 CPR resolution and a range of 7500 rpm. The location of the encoders is represented in Figure 6.1c.

6.1 eSEA modeling

The robotic actuator dynamic equation is given by the equation below, assuming the flexibility of the joint (K_e) as linear and the friction (F) as a function of the angular velocity ($\dot{\delta}$)

$$\begin{bmatrix} J & 0 \\ 0 & I \end{bmatrix} \begin{bmatrix} \ddot{\delta} \\ \ddot{\theta} \end{bmatrix} + \begin{bmatrix} K_e & -K_e \\ -K_e & K_e \end{bmatrix} \begin{bmatrix} \delta \\ \theta \end{bmatrix} + \begin{bmatrix} F(\dot{\delta}) \\ 0 \end{bmatrix} = \begin{bmatrix} \tau \\ 0 \end{bmatrix} \tag{6-1}$$

where δ, $\dot{\delta}$, $\ddot{\delta}$ are the motor's angular position, velocity, and acceleration, while θ, $\dot{\theta}$, and $\ddot{\theta}$ the link's. The known constants of the eSEA are the motor's moment of inertia $J = 0.0001\, m^4$, the link's moment of inertia $I = 0.0014\, m^4$, and the elastic constant of the flexible joint $K_e = 8.459\, Nm/rad$. The excitation input of the system is the torque of the motor represented by τ.

In the previous part, the different friction models used in this work were presented, combined with identification approaches the parameters are optimized to improve the accuracy of the models. In this assembly, the main source of friction can be found in the contact between the motor shaft and the elastic joint, given the relative displacement between the two.

6.2 Data Acquisition

The computer and the eSEA assembly communicate through the open-source *Odrive* board. The control flow chart is presented in Figure 6.2. The chart shows that the computer and the Odrive board communicate using the *Python* programming language. The Odrive sends the torque signal (τ) to the motor and obtains the angular measurements from the encoders where δ and θ are the motor shaft and the link's angular position, respectively. The *Odrive* board calculates the velocities and sends the values to the computer.

Although all three contributions focus on the same eSEA assembly, each focuses on a different aspect of the system. Before every experiment, the *Odrive* board calibrates and synchronizes the encoders and the motors. The experiment's time and signal vary depending on the case study and the studied phenomena. A PD position controller was implemented in an external loop to perform closed-loop experiments. The experimental data were recorded at a 500 Hz sample rate.

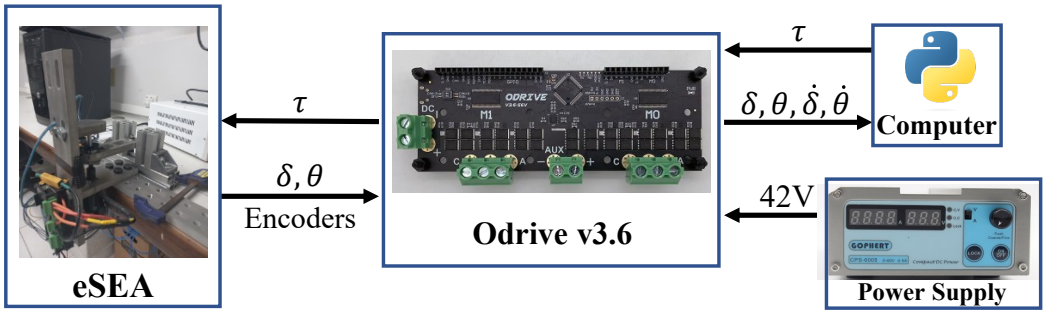

Figure 6.2: Control flow chart.

Part IV

Contributions

7
Nonlinear identification of an elastic joint of an elastomer-based series elastic actuator

SEAs have played an important role in developing human-interactive robots. Adding a compliant element to the joint offers advantages such as shock tolerance and passive energy storage, contributing to the safety of the interaction. Considering this, the present case study aims to model the dynamics of an original elastomer-based SEA (eSEA). The proposed approach compares the performance of three models in characterizing the dynamics of the eSEA's elastic joint. The linear model is an ARMAX model, the nonlinear is a NARX-ANN, and a hybrid model is proposed. The results showed that the proposed hybrid model decreases the MAE error of the ARMAX model by 93.0% and outperformed the NARX-ANN model, indicating its capacity to be used for modeling and control purposes.

7.1
Problem Description

The development of robotics over the past decades has made important advancements, especially involving human-robot interaction, including rehabilitation and assistance through exosuits [100]. Traditionally, classical robotics has prioritized stiff actuators due to their ability to achieve stability, high precision, and bandwidth of position control [35]. When human interaction is involved, stiff actuators can pose a safety issue [101]. SEA can solve this issue by providing joint compliance through an elastic element between the motor shaft and the link [102]. Robotic joint compliance offers advantages such as shock tolerance, high force control accuracy, and passive energy storage [36, 37]. These characteristics allow for better human-robot interaction control with mechanical compliance [103].

Multiple nonlinearities must be modeled in rigid joints, including friction, gear backlash [35]. In the case of SEA, new nonlinearities related to the compliant element flexibility must be considered. Model-based controllers have shown better performances for high-accuracy robots than regular controllers, requiring more accurate dynamical models [104]. With that in mind, using system identification methods to design better and more precise dynamic models has become essential.

In this contribution, three identification approaches are proposed using experimental data from an original experimental manipulator equipped with

an originally designed, adaptable, and low-cost eSEA. The first two models are linear and nonlinear algorithms, and lastly, an original hybrid model combining the ARMAX and NARX-ANN models. When comparing the performance of the three models using graphical plots, comparing the experimental data with the predictions and the validation metrics presented in Section 3.4, one could notice that all three models obtained adequate capacities for modeling the nonlinearities of the assembly. Nevertheless, it is observed that the hybrid model improved the performance of the original ARMAX model by 88.6% when using the RMSE metric and had the overall best performance with a determination coefficient of 0.999.

7.2 Data Acquisition

The focus of this work is to study the flexible joint. With that in mind, the link of the eSEA, described in Chapter 6, is restricted from moving, being held still using a metallic structure. The setup can be observed in Figure 7.1.

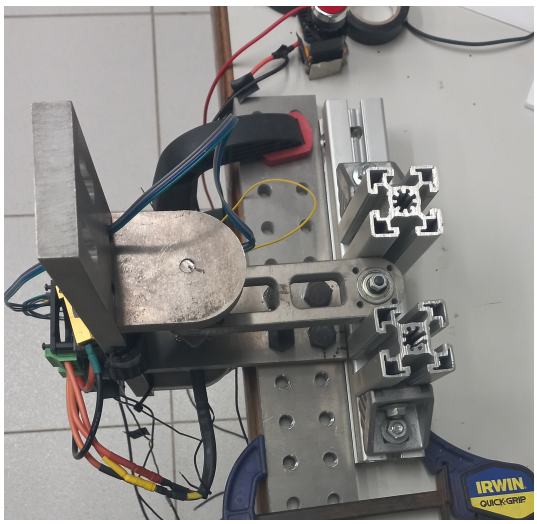

Figure 7.1: Assembled eSEA with the link held still.

The flexible joint is modeled using angular displacement measurements. The angular displacement is the difference between the angular position of the motor shaft and the link while the link is held still.

The torque excitation signal chosen for the identification is the swept sine or chirp signal. One of the advantages of this signal is the option to specify the magnitude and range of the frequencies. The torque frequency increases from 0 to 1 Hz over 43 *seconds* within an amplitude of 0.4 Nm. Both the input (torque) and the output (angular displacement) are plotted in Figure 7.2.

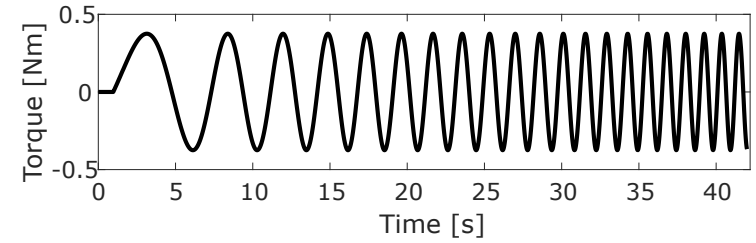

(a)

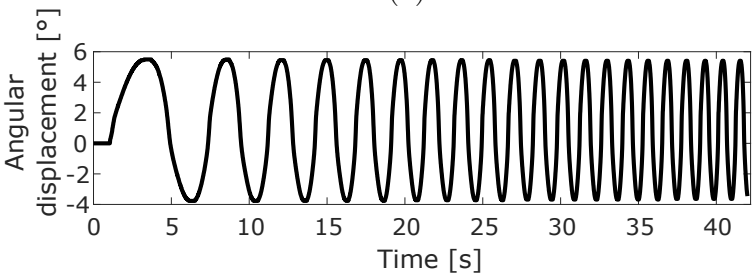

(b)

Figure 7.2: Plots of (a) Input torque (b) Angular displacement of the elastic joint of the eSEA assembly.

7.3 Proposed Approach

This work employs three identification methodologies. All three models are trained and validated using the same measured data, which is normalized. The first model used is the ARMAX model, presented in Section 3.1.1 Through hyperparameterization, the orders of the model are optimized, and the following orders are obtained: $n_a = 5$, $n_b = 5$, and $n_c = 3$. The linear model uses an identification package on R presented in [105].

The second model is the NARX-ANN model, described in Section 3.1.2. The following parameters were chosen through trial and error and hyperparameterization: 3 hidden layers containing 16, 32, and 64 neurons each, respectively. The other parameters regarding the model include $n_u = 2$, $n_y = 3$ model delay orders, *ReLu* activation function, *Nadam* optimizer, and a 1×10^{-3} learning rate. The training process was performed over 400 epochs with a batch size of 32, using the *Keras Python* package.

The last identification approach is a hybrid model combining the ARMAX and an ANN. The same ARMAX model of the first approach is used. However, the output of the ARMAX and excitation torque are used as input for an ANN to optimize and correct the ARMAX predictions. The ANN's inputs are the previous predictions and the input torque, and it is composed of 2 hidden layers with 32 and 64 neurons. The model orders chosen are $n_u = 2$ and $n_y = 2$. With the *ReLu* activation function, the *Adam* optimizer, and 1×10^{-3} learning rate, the training process was performed over 700 epochs

using a batch size of 32.

7.4 Results

This section presents the results of the proposed approach. Only the FR predictions of the validation dataset are used for the evaluation, and the different methods are compared through graphical and validation metrics.

The estimation of the angular displacement of the elastic joint of the eSEA assembly of all three models is plotted in Figure 7.3. Where the black line represents the measured data, and the red line the predictions of the model.

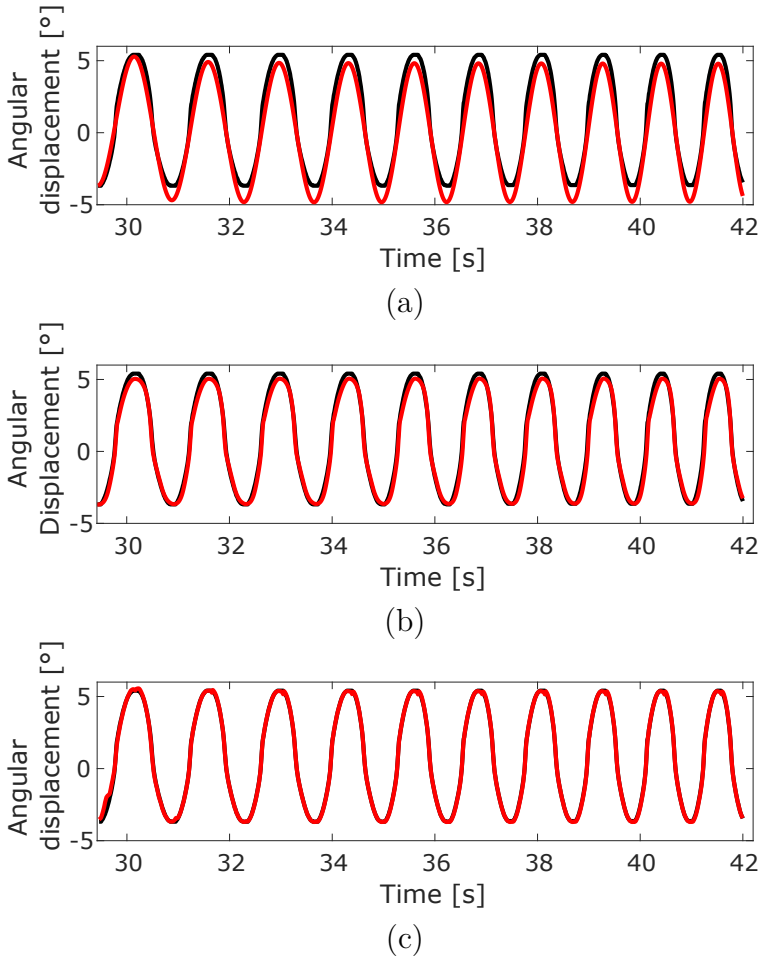

Figure 7.3: Result comparison between (a) ARMAX (b) NARX-ANN (c) ARMAX-ANN model and the experimental data. The model estimations plotted in red and the experimental data in black.

The ARMAX model, represented in Figure 7.3a, is a close fit to the experimental data. Characterizing the angular displacement and understanding the dynamics without the desired accuracy, especially at the peaks. The NARX-ANN performance is considerably better, following the measured data with higher precision than the previous model. Considering this model must be

precise, the ARMAX-ANN model, shown in Figure 7.3c, shows the best performance when analyzing the plots with almost no deviation from the measured data.

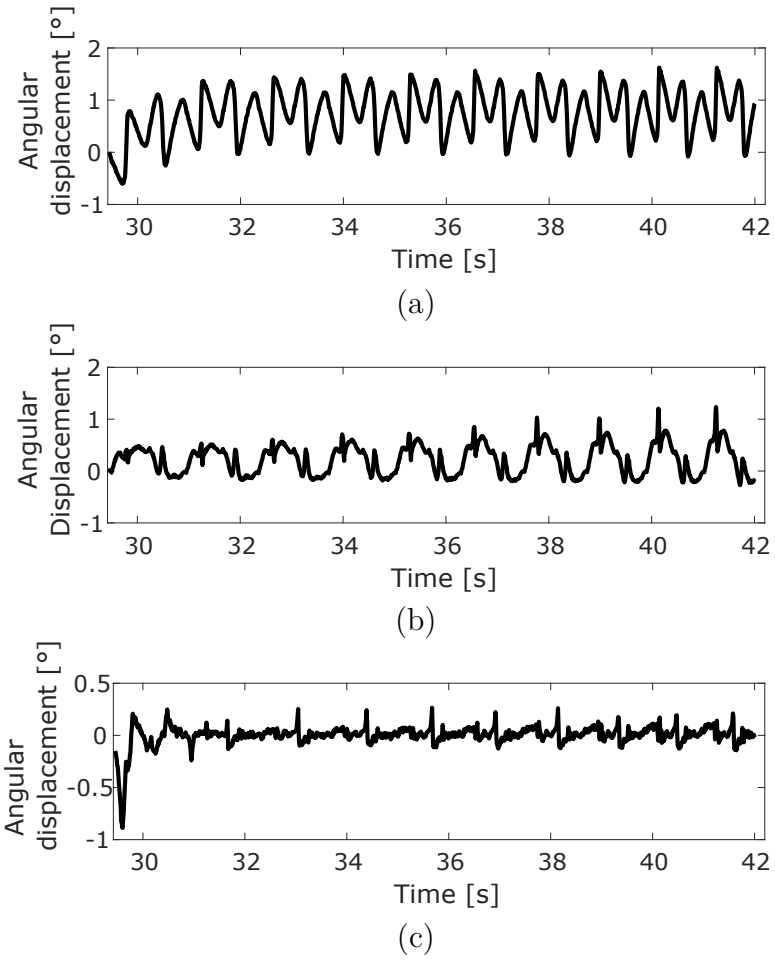

Figure 7.4: Error between (a) ARMAX (b) NARX-ANN (c) ARMAX-ANN model and the experimental data.

These observations are confirmed when comparing the error plots of the models, shown in Figure 7.4. The NARX-ANN errors are contained between -0.3° and 1.3° and increase when the frequency of the input torque is higher. The error of the ARMAX-ANN is consistently smaller and more stable, indicating a better fit to the experimental data. After an initial deviation, the error stabilizes between -0.2° and 0.3°, indicating a significant improvement in performance predictions compared to the original ARMAX model. This suggests that combining the ARMAX and ANN approaches can lead to more accurate predictions in this case.

Figure 7.5 displays the correlation plot of the three models. The plot considers the proximity of the scattered points to the ideal model represented by the dotted line. With that in mind, the ARMAX model shows the poorest performance. Comparatively, the performance of the NARX-ANN predictions

indicates a good capacity to predict the dynamics of the eSEA. Adding the ANN to the ARMAX model considerably improves the model, showing the closest predictions to the ideal model.

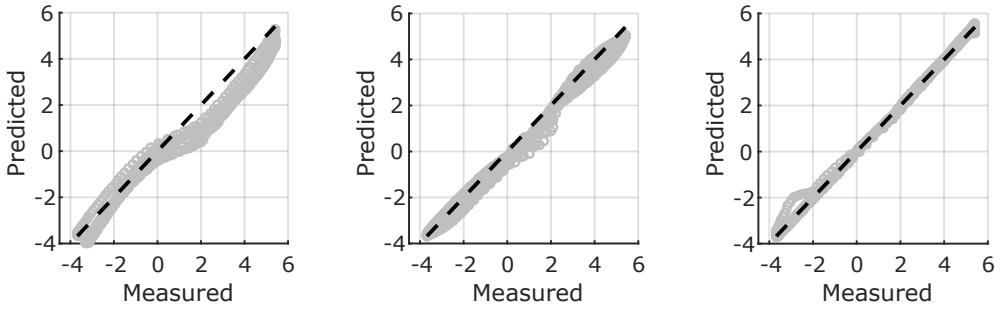

(a) (b) (c)

Figure 7.5: Correlation between the (a) ARMAX (b) NARX-ANN (c) ARMAX-ANN predictions and the experimental data.

Table 7.1: Validation metrics of the eSEA identification

Model	Type	R^2	*RMSE*	*MAE*	F%	V%
ARMAX	Train	0.939	0.872	0.771	75.86	98.64
	Validation	0.939	0.868	0.767	75.84	98.37
ANN	Train	0.993	0.296	0.229	91.60	99.63
	Validation	0.989	0.363	0.296	89.69	99.34
ARMAX-ANN	Train	0.999	0.0429	0.0248	98.76	99.98
	Validation	0.999	0.0989	0.0537	97.18	99.92

Table 7.1 presents the validation metrics presented in Section 3.4. Comparing the error metrics confirms the previous observations of the graphical analyses. All three models characterize the dynamics of the elastic joint with varied success. This can be observed by the coefficients of determination higher than 0.9 for all three models, a satisfactory result depending on the application.

One can notice that the FIT% and the VAL% of the NARX-ANN predictions are higher than 90%, showing satisfactory prediction ability compared to the ARMAX model. The model showing the best ability to characterize the eSEA is the ARMAX-ANN model, decreasing the test ARMAX model *RMSE* and *MAE* errors by 88.6% and 93.0%, respectively. Moreover, the ARMAX-ANN model shows a coefficient of determination close to 1 and the lowest errors. This shows a significant improvement compared to the initial ARMAX model.

7.5 Discussion

By adding a compliant element to the eSEA assembly, a new nonlinear phenomenon must be considered. This behavior was studied extensively in this identification work.

The linear model showed its limitations when characterizing the angular displacement of the joint. Compared to the other models, the ARMAX obtained the highest errors. In human interactive applications, the model is not precise enough to be used in a model-based controller.

The second model improved significantly compared to the linear model, which is expected considering that ANN has a greater capacity for representing nonlinearities and other complexities, lowering the $RMSE$ error by 65.87% and improving the FIT metric considerably. The NARX-ANN model accuracy can be noticed in the correlation graphics in Figure 7.5. The model accuracy shows the model could be used for most applications.

Nevertheless, the hybrid model addressed the system's unmodelled nonlinearities. The most accurate predictions was obtained by adding an ANN to the linear model, reflecting the ANN's ability to correct the difference between the original ARMAX and the measured data.

This contribution aimed to study and obtain an accurate model for the flexible joint of an eSEA assembly. The study was conducted using three different approaches. The proposed hybrid model combines an ARMAX and an ANN. This model showed the most accurate prediction. The proposed approach could easily be used and trained in other highly nonlinear systems.

8
Physics-informed and black-box identification of a robotic actuator with a flexible joint

Acquiring an accurate model characterizing a robotic system's dynamics can be challenging and necessary considering the safety and functionality impacts.One of the alternatives to address this issue is system identification, which aims to obtain models through physical and experimental observations. In this manner, the developments in ML algorithms, such as novel neural networks, have significantly improved the modeling of complex and nonlinear phenomena. This contribution focuses on examining the performance of the PINNs for the identification task, estimating the parameters of 4 friction models utilizing PINNs. The performance is compared to two black-box models. The experimental data used is from original eSEA assembly presented in Section 6. The PINNs outperformed the black-box models. The friction model that best represented the robotic actuator was the LuGre model, with the parameters obtained using the PINNs outperforming the best black-box model by lowering the MAE by 30.83%. With a determinant coefficient of 0.94, the model shows a high capacity for describing the multiple nonlinearities present in the system.

8.1
Problem Description

ML advancements have significantly impacted system identification with new algorithms, training methods, and hardware. In the past years, a new wave of solutions using neural networks has appeared, significantly improving black-box identification. These are generally easier to implement and obtain accurate results, but they lack interpretability and generalization capacities when using the model for a different system, when compared to white-box approaches [16, 46].

Some fields, such as criminal justice, finance, and medicine, do require some interpretability [51]. Therefore, gray-box modeling is often used to optimize and augment the accuracy of a model while maintaining interpretability by estimating the parameters of physics-based models. Physics-informed neural networks (PINNs) are an example of gray-box modeling. Introduced in [56], this innovative algorithm has shown promising results in parameter identification.

This study focuses on the applications of such algorithms in robotics.

Through this idea, this work studies the efficiency of the PINNs for the identification task of friction parameters of an easy assembly. The main contribution of this work is to test the performance of the PINNs for a highly nonlinear and complex original low-cost eSEA benchmark.

8.2 Data Acquisition

The case study used in this work is the eSEA assembly described in Section 6. The following excitation signal is used in this identification task. Figure 8.1 presents the input and output, showing the swept-sine torque signal, with a torque frequency increase from 0 to 1 Hz over 8 *seconds* within an amplitude of 0.2 Nm.

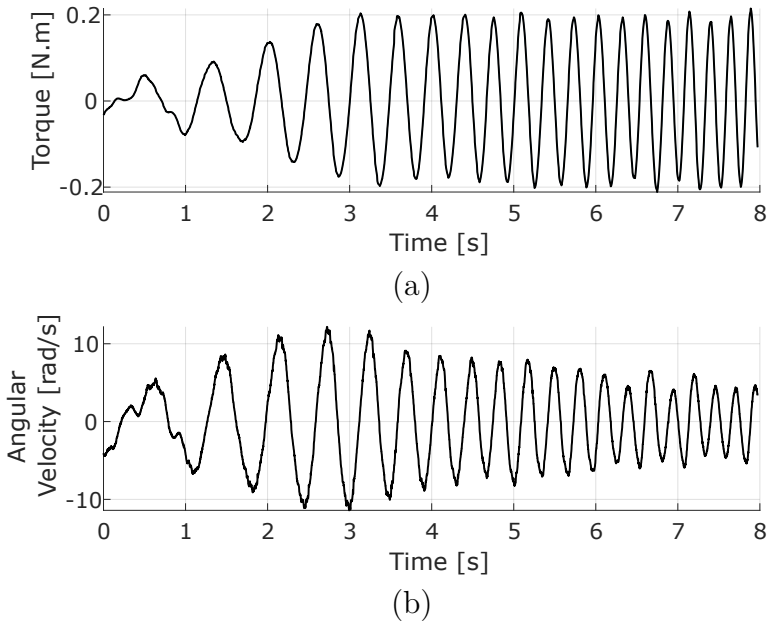

Figure 8.1: Plots of (a) Input torque (b) Angular displacement of the elastic joint of the eSEA assembly.

8.3 Proposed Approach

In this work, the performance of two black-box models and a gray-box model are compared. The black-box models are both the ARX and the ARMAX models; both are variations of the ARMAX model presented in Section 3.1.1. The ARX model is defined by the following:

$$A(q)y(t) = B(q)u(t - n_e) + e(t) \tag{8-1}$$

The ARMAX is given by:

$$A(q)y(t) = B(q)u(t - n_e) + C(q)\xi(k) + e(t) \tag{8-2}$$

Both linear models are implemented in MATLAB using the System Identification Toolbox. The identification task initially involves defining the model's lags and orders. By the process of hyperparametrization, the following lags are obtained:

- **ARX**: $n_a = 10$, $n_b = 10$, $n_e = 10$.
- **ARMAX**: $n_a = 5$, $n_b = 2$, $n_c = 2$, $n_e = 1$.

The PINNs model is used as the gray-box model. A few parameters and equations describing the assembly must be defined, as mentioned in the description of the PINNs model, given in Section 3.2.

First, considering the work focuses on the eSEA assembly, the ODEs of the model dynamics must be chosen; these equations are given in Section 6. Table 8.1 shows the parameters that must be identified for each friction model. One could notice the LuGre and the Coulomb-Stribeck have the most parameters, making the identification task more challenging.

Table 8.1: Parameters of the friction models of the eSEA.

Parameter	Linear	Coulomb-Stribeck	Dahl	LuGre
f_v	X	X	-	X
f_c	-	X	X	X
f_s	-	X	-	X
$\dot{\delta}_{Stribeck}$	-	X	-	X
σ_0	-	-	X	X
σ_1	-	-	-	X

As mentioned in the definition in the Background Theory chapter, the training of PINNs is divided into two parts. The first training focuses on making the DNN characterize the system's state dynamics. With time (t) and the excitation torque (τ) as input, the angular position of the motor shaft and the link are estimated. The DNN comprises four hidden layers with 128 neurons each and the *tanh* activation function. The initial training is over 400,000 epochs, with a learning rate of 1×10^{-3} and the *Adam* optimizer.

Following the initial training, the PINNs add the friction parameters and the additional conditions to the loss function, allowing for the optimization of the friction parameters and performing the gray-box identification task. The training is done over 200,000 epochs, with a learning rate of 1×10^{-4} and the *L-BFGS*, a second-order optimizer.

The results of both these models are presented in the next section.

8.4 Results

In the following, the results obtained by applying the proposed approach to the eSEA are presented. The validation dataset is used to evaluate the performance of the models.

8.4.1 Black-box Identification

Figure 8.2 shows the ARX and the ARMAX model plots compared to the measured data, represented by a dotted red line and a blue line, respectively.

The ARX model exhibits a strong correlation with the measured data, particularly in the mid-range of angular velocities. However, it overestimated velocities at higher magnitudes and underestimated them at lower magnitudes. These observations are confirmed when looking at the error plot in Figure 8.3a.

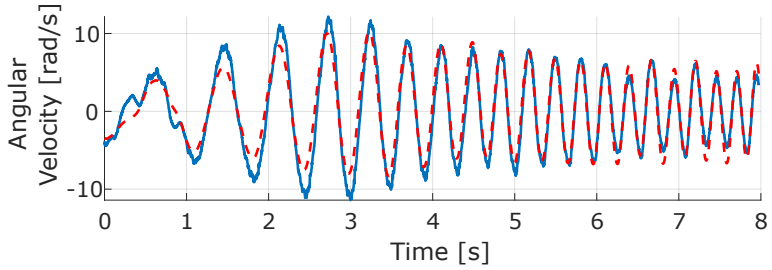

(a)

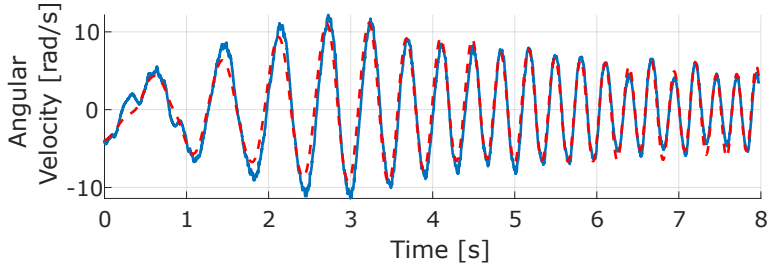

(b)

Figure 8.2: Correlation between (a) ARX (b) ARMAX model and the experimental data. The model estimations plotted in red and the experimental data in blue.

However, compared to the ARMAX model, the latter demonstrates a good fit to the measured angular position, with minimal deviations. In fact, the model shows deviations when trying to capture the extremes accurately, especially during rapid velocity changes. The error plots provide additional insight when comparing the estimations.

The graphical analysis is confirmed when analyzing the validation metrics in Table 8.3. A coefficient of determination (R^2) close to 1 indicates a better

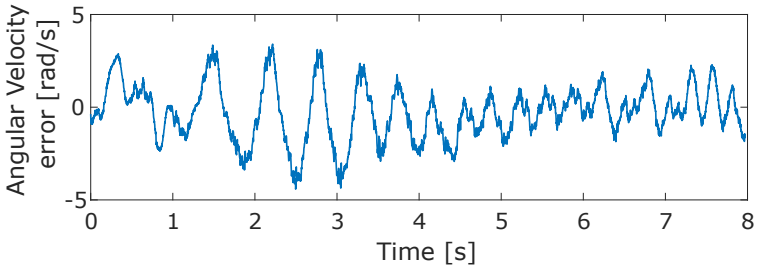

(a)

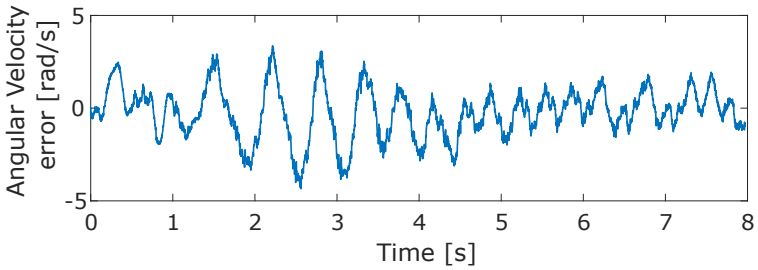

(b)

Figure 8.3: Error between (a) ARX (b) ARMAX and the experimental data.

fit between the model and the data. The ARMAX model shows a higher R^2 (0.912) than ARX (0.897). Actually, the ARMAX model outperformed the ARX model in every metric, with the highest difference being the RMSE, with a 10.43% reduction.

8.4.2 PINNs

The estimated parameters of the eSEA were obtained using the PINNs algorithm. The parameters are presented in Table 8.2.

Table 8.2: Estimated Parameters of the eSEA.

Parameter	Linear	Coulomb-Stribeck	Dahl	LuGre
f_v	0.00963	0.002	-	0.00335
f_c	-	0.0145	0.0379	0.01619
f_s	-	1.03×10^{-5}	-	0.8795
$\dot{\delta}_{Stribeck}$	-	0.1677	-	3.15×10^{-5}
σ_0	-	-	0.5034	0.0512
σ_1	-	-	-	0.0036

Using the estimated parameters and the ODEs equations, presented in Section 6.1, the system is simulated. Figure 8.4 shows the performance of all four models where the blue line represents the measured data from the assembly, and the dotted red line represents the estimation from the model.

Considering the linear model exhibits a simple relationship between the torque and velocity, the model shows a decent correlation with the experimental data. The main differences occur in the extremes where the transient behavior occurs and when the friction is the most nonlinear.

The Coulomb-Stribeck model adds more elements, including static friction and the Stribeck velocity. Given that, the performance obtained is worse than expected. With similar performance to the linear model when analyzing the model results graphically (Figure 8.4b).

The Dahl model adds a new state to the linear model, considering z as the elastic deformation. With these additions, phenomena such as zero slip displacement and hysteresis are captured. Graphically, it is possible to observe the important error in the initialization of the ODEs due to the instability of the new state z. After the initialization, the model shows its limitation in capturing the complex friction phenomena, with constant errors and difficulty in modeling the transient phase of the angular velocity. The error plot (Figure 8.5) shows the Dahl model has the highest errors out of all the friction models.

Lastly, the LuGre model is the most sophisticated model that combines elements from previously mentioned models, considering effects such as stiction, stick-slip, Stribeck, hysteresis, and zero slip displacement. Through this process, the LuGre friction model provides the best overall fit for the experimental data, capturing precisely both the transient and the steady-state behavior. The error plots represented in Figure 8.5d confirm the previous observation, where the errors were significantly reduced compared to the other models, especially in the peaks of the angular velocity.

8.4.3 Result discussion

In order to appropriately evaluate and compare the performance of the models the validation metrics are used. Table 8.3 shows the performance of the four friction models obtained using the PINNs. The error metrics are calculated by comparing the estimations with the measured data. The Linear, Coulomb, and Dahl models show a relatively low performance with RMSE and MAE errors higher than the ARX model, suggesting less accuracy when characterizing the system. The best friction model is the LuGre model. The LuGre model outperforms all the other models across all the metrics. Exhibiting the highest R^2, with 0.94, which is very close to an ideal model, and an RMSE error of 1.31, which is a 24.27% reduction compared to the next-best gray-box model. And showing the highest FIT and VAF percentages. This result is expected, given that the LuGre friction model considers the highest

amount of phenomena characterizing friction.

Through these results, one could notice the friction is an influential phenomena in the eSEA assembly that must be modeled. The main friction source can be attributed to the contact area between the motor shaft and the joint. The most challenging period to model is the beginning of the movement or the change of directions, or the static phase. Following that, friction tends to stabilize. Considering the rotational excitation torque changes frequently, the change of direction makes the friction a challenging phenomena to model. With that in mind, from the chosen friction models the LuGre model is the best at modeling both the static and dynamic phases of the friction.

Considering that both the ARMAX and the LuGre friction models show similar performances, with the gray-box model edging it by a small margin. Other aspects of each methodology must be taken into account. As discussed in the introduction, the LuGre model's significant advantage is interpretability, being an equation-based model that allows for the easy implementation of a model-based control approach.

Table 8.3: Evaluation Metrics of the eSEA identification.

Model	R^2	RMSE	MAE	FIT	VAF
ARX	0.897	1.61	1.27	68.05	90.66
ARMAX	0.912	1.49	1.15	70.49	91.99
Linear	0.898	1.73	1.38	68.13	89.99
Coulomb	0.884	1.85	1.49	66.00	88.59
Dahl	0.874	1.93	1.52	64.74	88.58
LuGre	0.942	1.31	1.03	75.93	94.86

8.5 Discussion

This work focused on comparing the identification performances of black-box and gray-box models. The black-box identification used ARX and ARMAX models, while the gray-box used PINNs for the friction parameter estimation and used the known ODEs to simulate the model. The models were evaluated through several evaluation metrics, with both methods showing adequate performances to model the dynamics of the systems.

Both the black-box and the gray-box identification of the eSEA showed a good fit compared to the measured data. ARMAX is the best black-box model, with an $R^2 > 0.9$ and a good capacity at capturing the trend of the system when analyzing using the graphical plots.

The PINNs demonstrated their capacity to optimize parameters in a gray-box identification context. All four friction models obtained a high coefficient of determination (>0.87). The friction model with the best performance is the LuGre model, having the lowest errors and best validation metrics. Adding to the overall better performance of the PINNs model, the element of interpretability plays a role in its favor.

Future works shall focus on the potential use of the identified model for model-based control. These works also include testing the PINNs using other assemblies with higher degrees of complexity.

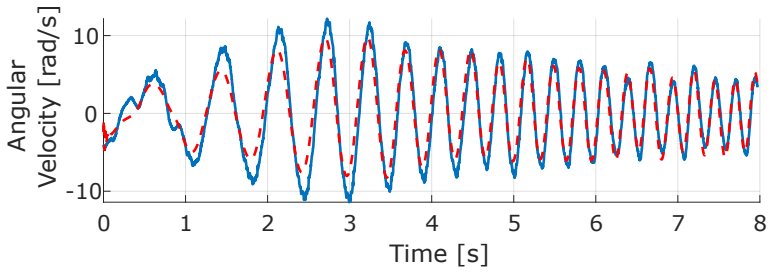

(a)

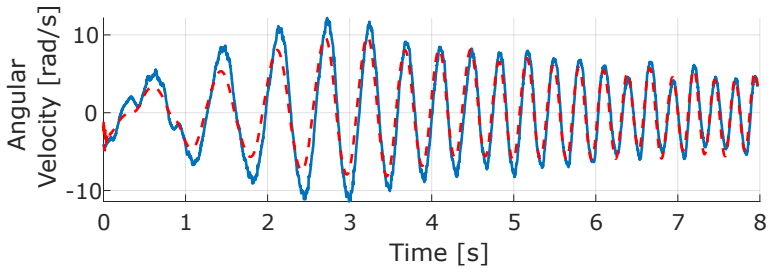

(b)

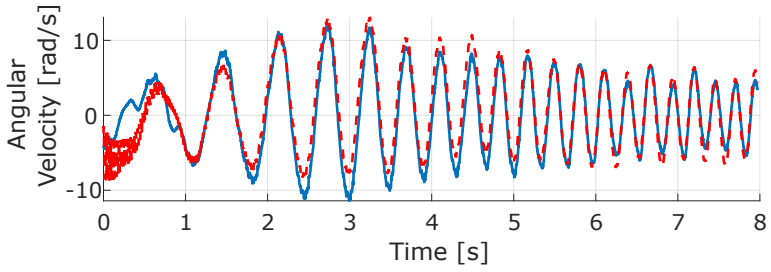

(c)

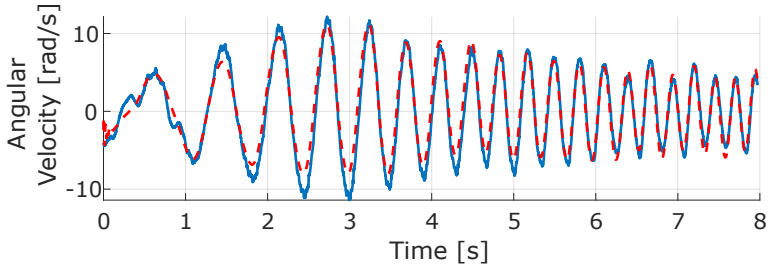

(d)

Figure 8.4: Correlation between the identified (a) Linear (b) Coulomb (c) Dahl (d) LuGre friction models and the experimental data. The model estimations plotted in red and the experimental data in blue.

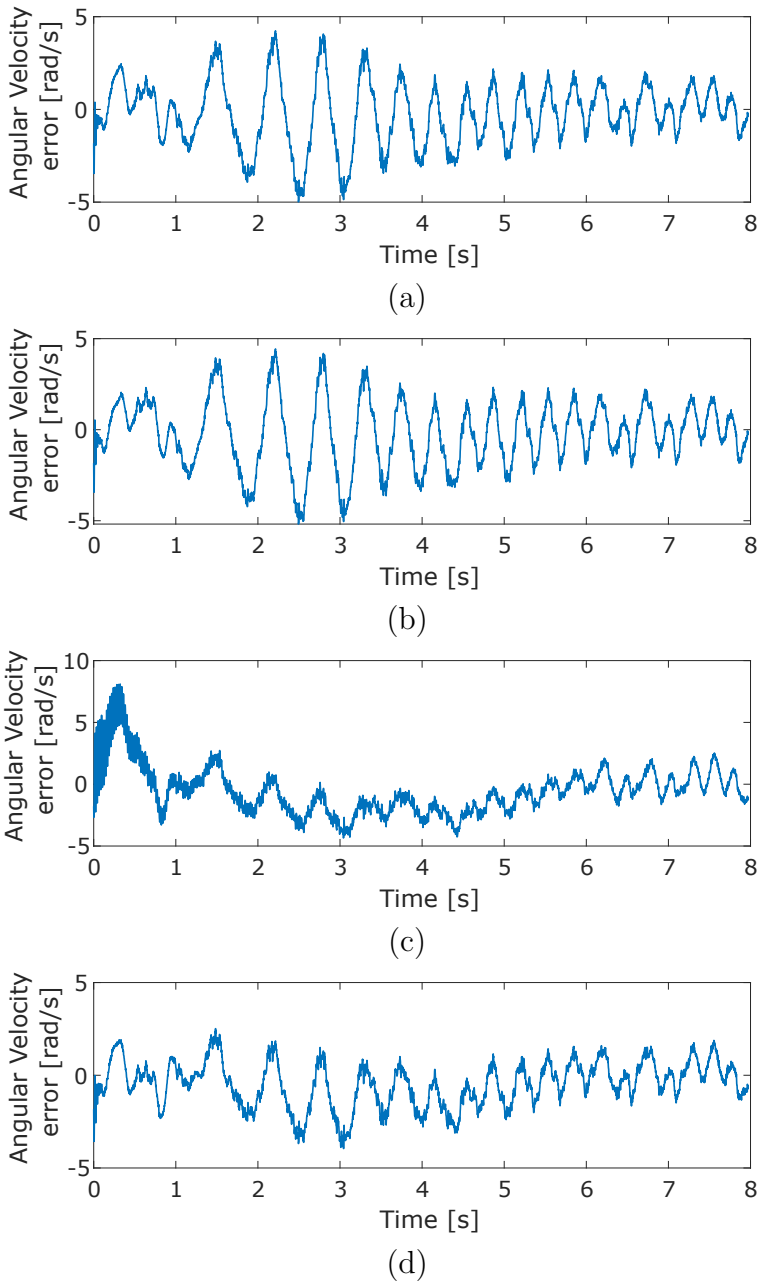

Figure 8.5: Error between the identified (a) Linear (b) Coulomb (c) Dahl (d) LuGre friction models and the experimental data.

9
Identification of the friction model of a single elastic robot actuator from video

In robotics, precise models are constantly needed to optimize the performance and safety of these systems. Thanks to the developments in ML, algorithms such as CNNs have performed well in extracting features from images. Techniques like TL can lower the computational cost and optimize the training task. Through these processes, this contribution aims to obtain a dynamic model from video data. This work aims to perform the gray-box identification of friction parameters using experimental data from an eSEA assembly. The proposed model is composed of three parts. The first employs pre-trained CNNs and Transfer learning to estimate the states of an eSEA assembly. Following that, an LSTM is added to estimate the velocity and acceleration of the system. Lastly, the states are used to optimize the friction parameters.

9.1
Problem Description

In industry, robotic manipulator applications have required accurate dynamic models for safe operations and optimal performance in precision tasks, especially in the case of collaborative robots [106]. One element that impacts performance and has shown to be challenging to model accurately is friction due to its highly nonlinear nature [91, 107]. Many models have been proposed, but most have not shown to be ideal when implemented due to the high number of phenomena involved [108]. Moreover, recent publications show the subject maintains its relevancy [109–111].

A solution that has shown accurate results has been system identification, which has been Implementing various nonlinear algorithms to find black-box and gray-box solutions to complex systems within multiple fields [44]. The advancements in ML have significantly contributed to improving system identification performances, facilitating the modeling of more complex systems with multiple nonlinearities and high-dimensional data such as images [17].

A novel methodology for performing vision-based parameter estimation of mechanical systems, specifically an actuator with a flexible joint, is proposed. With interpretability in mind, the proposed approach allows to make the gray-box identification and optimize physical parameters from existing models through video, by combining a black-box algorithms with a gray-box algorithms. The black-box approach conducts the state estimation (position,

velocity, and acceleration) of the actuator from data frames using both CNN and LSTM architectures, with the help of transfer learning to facilitate the training process. Following that, the layers are frozen, and the dynamic equations layer is added to perform the gray-box identification of the friction parameters (such as viscous, Coulomb, static friction coefficients, and the Stribeck velocity) using the estimated states and the ODEs of the system, which are fixed.

9.2 Proposed Approach

The main goal of this work is to estimate an eSEA assembly's friction parameters. The following section presents the proposed approach's three steps. The first two steps involve estimating the robotic actuator's pose, velocity, and acceleration using pre-trained deep CNNs with TL and LSTM architecture. Lastly, a physics-informed layer with the hard-coded ODE is added to the model to perform the friction parameter identification.

The torque excitation signal chosen for the identification procedure was the sine signal. The sine signal has an amplitude of 0.09 Nm and a frequency of 10 Hz over 40 *seconds*. This signal allows us to specify the magnitude and frequencies used to excite the system and has shown satisfactory results in identification problems.

Compared to the other contributions, the experiment is filmed using a

With the objective of using the videos to measure the movement of the link, a Sony α6400 camera is used to record the experiment with a constant recording frame rate of 120 frames per second. With the intent to synchronize the camera recording and the encoder measurements, an Arduino controlling an LED light turns on when the algorithm starts, as can be seen in Figure

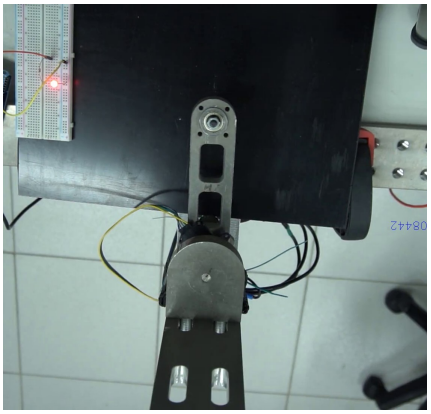

Figure 9.1: Frame of the video of the eSEA assembly used for the training of the CNN.

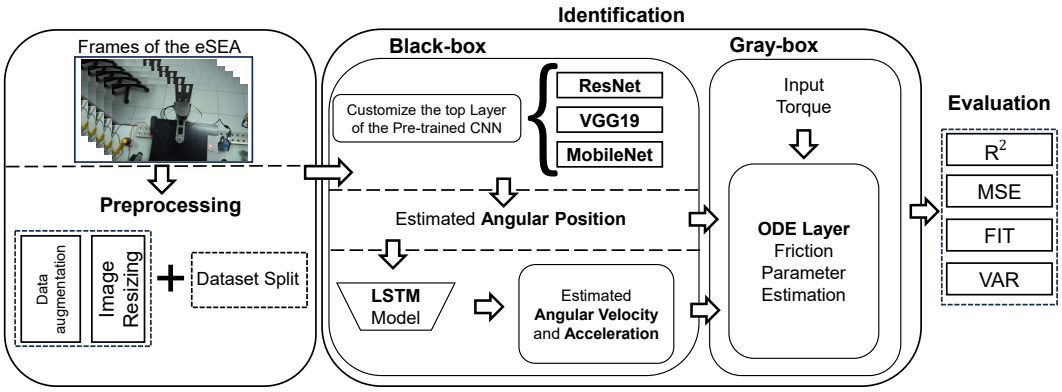

Figure 9.2: Proposed approach diagram.

9.2. Due to the difference in sampling rates between the camera and the encoders, a resampling is required to match each frame with a measurement using MATLAB.

9.2.1 Pose Estimation

This step aims to estimate the link's angular position and the original actuator's motor shaft using the video frames. In order to extract information from images CNNs are used, an architecture adapted to process multidimensional arrays, described in Section 4.2. Table 9.1 shows the characteristics of the models chosen, including the number of layers and parameters that must be trained for each model. The floating point operations per second (FLOPS) of each model are given in G, or 10^9 operations per second, showing a correlation between the FLOPS of each model and the number of parameters. Lastly, the performance of each model in the ImageNet benchmark indicates the accuracy in the classification of images.

Table 9.1: Description of the CNNs

Model	Number of Layers	Parameters in Millions	FLOPS $[G]$	ImageNet Top 1 [%]	ImageNet Top 5 [%]
MobileNetV2	53	3.50	0.30	71.89	90.29
Densenet121	121	7.98	5.69	74.43	91.97
EfficientNetB0	237	5.29	0.39	77.69	93.53
ResNet101	347	44.55	7.80	77.37	93.55
VGG19	46	143.67	19.63	72.38	90.88

As one can notice, each CNN has millions of parameters that must be optimized, which can be highly computationally costly and require an immense amount of data. Considering this, transfer learning becomes an

optimal solution to this problem by freezing the feature-extracting layers of the model and repurposing the trained CNN for our regression problem.

Initially, the model that offers the best performance at estimating the manipulator's pose must be chosen. All five models will be tested. Then, the three best models will be used for the following steps.

For all the CNN models, the weights and biases of all but the last convolutional layer are frozen, and the fully connected layer is replaced with a regression layer composed of 256, 128, 32, and 2 neurons. The input will be the video frames; the output is the link's xy coordinates.

The methodology is implemented using the *Pytorch* package. The training adopts a batch size of 64 over 100 epochs using the *Adam* optimizer with a 1×10^{-3} learning rate.

The video frames are cropped and resized to a 224×224 ratio, obtaining tensors of size (3,224,224), where 3 is the color aspect of the image. The angular positions are converted to x and y coordinates to facilitate the training process. The training proportions chosen in this work are 70% for training, 20% for validation, and 10% for testing.

9.2.2 Velocity and Acceleration estimation

The second step involves estimating the velocities and accelerations of the robotic actuator using the angular positions estimated using the pre-trained CNNs. By using the LSTM architecture and the sequence of angular positions with a chosen delay (n) as input. After trial and error, the ideal minimum and delay chosen is $n = 5$, meaning the LSTM architecture must be given a sequence of 5 angular positions to make the state estimations. By stacking the pose estimation CNN model, the model is able to process 5 frames and provide the necessary measurements for the LSTM network. The LSTM architecture is composed of 2 layers, 50 cells each, and with a *tanh* activation function.

The deep pose estimation CNN model is stacked; 5 frames are estimated simultaneously. The LSTM layers are added to the stacked CNN layers. The LSTM parameters are optimized using the same CNN training configuration after freezing all but the LSTM layer's weights. The inputs are 5 frames of the video, and the outputs are the angular velocities and accelerations of the motor and the link of the robotic actuator.

9.2.3 Gray-box Identification

The friction gray-box identification is implemented by adding a hard-coded layer representing the system's modeling equations. The eSEA assembly equations are given in Section 6.1.

Table 9.2: Range of the estimated parameters.

	Linear	Coulomb-Stribeck
f_v	$\{0.001 - 0.1\}$	$\{0.005 - 0.015\}$
f_c	-	$\{0.0045 - 0.15\}$
f_s	-	$\{0.0005 - 0.0015\}$
δ	-	$\{0.00375 - 0.0115\}$

Considering that the states of the robotic actuator have been obtained through the previous steps, a layer is added to the existing CNN-LSTM model describing the system's dynamics. The parameters to be optimized are the friction coefficients, presented with their respective search ranges in Table 9.2. Search ranges help the identification task considerably, helping the optimization process, and can easily be implemented using the *Pytorch* package.

9.3 Results

This section presents the results of the different steps of the identification. The first is the pose estimation using the five deep pre-trained CNNs. Following that, the velocity and acceleration estimations of the three best pose estimations CNNs are compared. Lastly, using the estimations obtained, the parameters of the two friction models are optimized and identified from the video frames.

9.3.1 Pose estimations

This section presents the results from the pose estimations using the five pre-trained CNNs. Table 9.3 shows the validation metrics of each model. The coefficient of determination measures the correlation between the measured data and the estimated position; the closest to 1, the better the model is. With that in mind, all models obtained highly accurate estimations.

In computer science, the model should be chosen based on its performance using the validation data. In this case, the model with the best performance is the VGG19, with a FIT of 93.89% and a VAF metric of 99.63%, showing a high

Table 9.3: Validation metrics of the models.

Model	Type	R^2	RMSE	MAE	F%	V%
MobileNet	Train	0.9927	0.0395	0.0317	91.44	99.27
	Valid	0.9928	0.0399	0.0315	91.48	99.28
	Test	0.9923	0.0404	0.0318	91.24	99.24
Densenet	Train	0.9826	0.0608	0.0461	86.83	98.27
	Valid	0.9899	0.0471	0.0370	89.96	98.99
	Test	0.9890	0.0483	0.0371	89.51	98.95
EfficientNet	Train	0.9930	0.0387	0.0307	91.62	99.30
	Valid	0.9922	0.0413	0.0325	91.20	99.38
	Test	0.9927	0.0393	0.0314	91.47	99.35
ResNet	Train	0.9908	0.0442	0.0353	90.42	99.08
	Valid	0.9928	0.0398	0.0327	91.51	99.31
	Test	0.9923	0.0403	0.0335	91.25	99.24
VGG19	Train	0.9956	0.0305	0.0246	93.40	99.58
	Valid	0.9963	0.0287	0.0234	93.89	99.63
	Test	0.9958	0.0300	0.0246	93.50	99.59

level of accuracy and a high correlation between the measured and estimated position. The MobileNet model is the second best performing model, even though it is the model with the fewest parameters (3.5 million parameters) or 2.43% of the number of parameters of the VGG19 model with a FIT and VAF metric values over 91%, indicating a good capacity for estimating the link's angular position from the images. With these results, the pre-trained models used for the next steps are MobileNet, ResNet, and VGG19.

9.3.2 Velocity and Acceleration estimations

The following results were obtained after adding the LSTM layer to the CNN models. Table 9.4 shows the validation metrics for the validation dataset. All three models show excellent results. With low errors and high R^2, the models effectively capture the states from the video frames. The best overall model is the VGG19, with the lowest MSE errors across most states.

Table 9.4: Metrics evaluating the performance of the TL models using the validation dataset

Model	Position		Velocity		Acceleration	
	R^2	MSE	R^2	MSE	R^2	MSE
MobileNetV2	0.990	0.002	0.959	0.887	0.972	60.900
ResNet101	0.992	0.002	0.969	0.667	0.970	66.268
VGG19	0.995	0.001	0.967	0.711	0.973	58.150

The plot of the best-performing model is shown in Figure 9.3. The blue line represents experimentally obtained data; the dotted red line represents the estimated state. Observing the plot, the state estimation can be considered more than adequate and highly accurate.

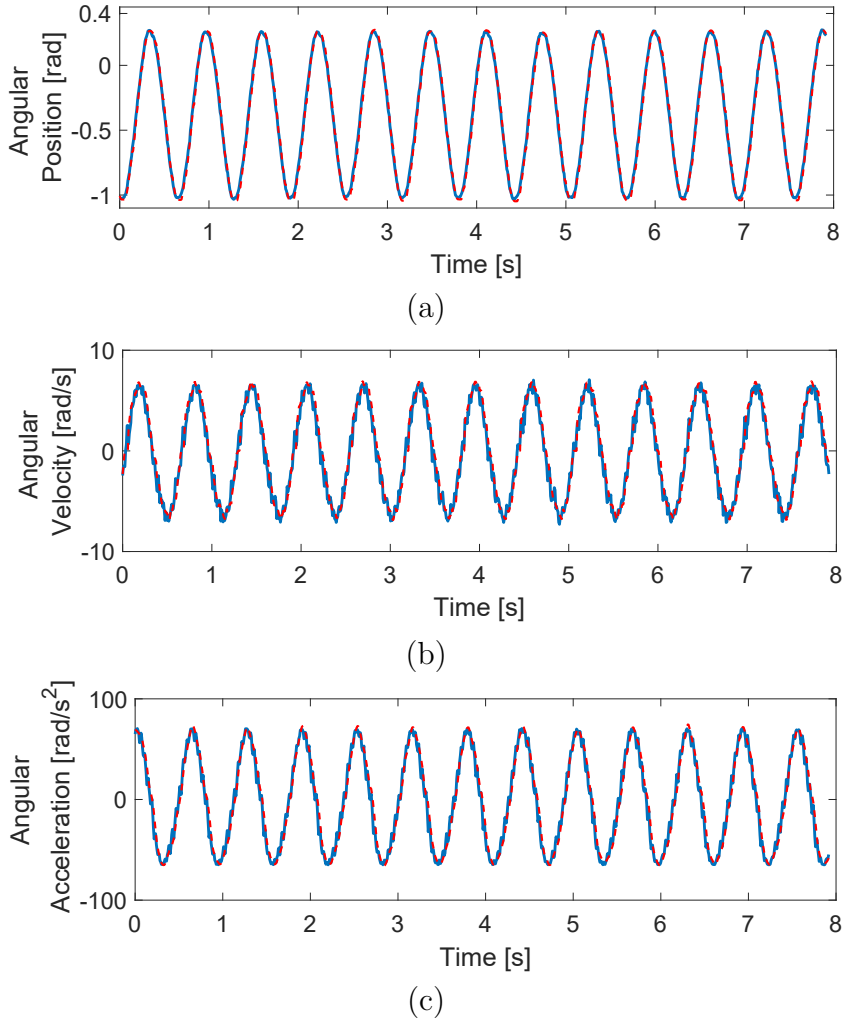

Figure 9.3: Correlation between the estimated angular (a) position (b) Velocity (c) Acceleration and the experimental data. The model estimations plotted in red and the experimental data in blue.

9.4 Gray-box Identification

After estimating the states of the robotic actuator from video data, the gray-box layer is added to the model. Table 9.5 shows the estimated parameters of the friction models.

The states are simulated using the ODE's and the estimated parameters. Table 9.6 shows the relation between the simulated and experimental link's angular velocity through validation metrics. Analyzing the metrics, the model

Table 9.5: Parameters Estimated using video.

Model	Linear	Coulomb-Stribeck
f_v	0.0033	0.0088
f_c	-	0.0083
f_s	-	0.0009
δ	-	0.008

showing the best performance is the Coulomb-Stribeck model. Having the lowest MAE and MSE errors in the validation and test datasets. Another metric indicating the excellent capacity of the model to characterize the eSEA is the VAF of 89.1%, showing a high correlation between the estimated and the measured angular velocity. This result is to be expected, considering the linear model considers the lowest amount of friction phenomena.

Table 9.6: Validation Metrics of the friction models.

Model	Type	R^2	MSE	MAE	FIT	VAF
Linear	Train	0.874	2.623	1.429	64.57	87.47
	Valid	0.886	2.366	1.380	66.23	88.60
	Test	0.877	2.642	1.420	64.96	87.93
Coulomb	Train	0.889	2.322	1.170	66.66	88.89
	Valid	0.890	2.283	1.166	66.83	89.01
	Test	0.891	2.338	1.181	67.00	89.12

The graphical analysis confirms the excellent performance of the Coulomb-Stribeck model. The angular measurement (in blue) is compared to the simulated estimation (in red). The error is between 2 and -2 rad/s, mainly in the extremes of the sine waves.

9.5 Discussion

The methodology shows an overall good performance. All three steps yield precise results. The VGG19 architecture combined with the LSTM presented precise state estimation of the eSEA, with a coefficient of determination higher than 0.95 for all the states, showing the potential of using the model as state-observers for system control.

From it, the parameters of two friction models are obtained. Through its ODEs and the estimated parameters, the simulation shows high fidelity to the measured data. The proposed approach shows its potential for gray-box identification using video data, showing the possibility of obtaining an interpretable model from video data.

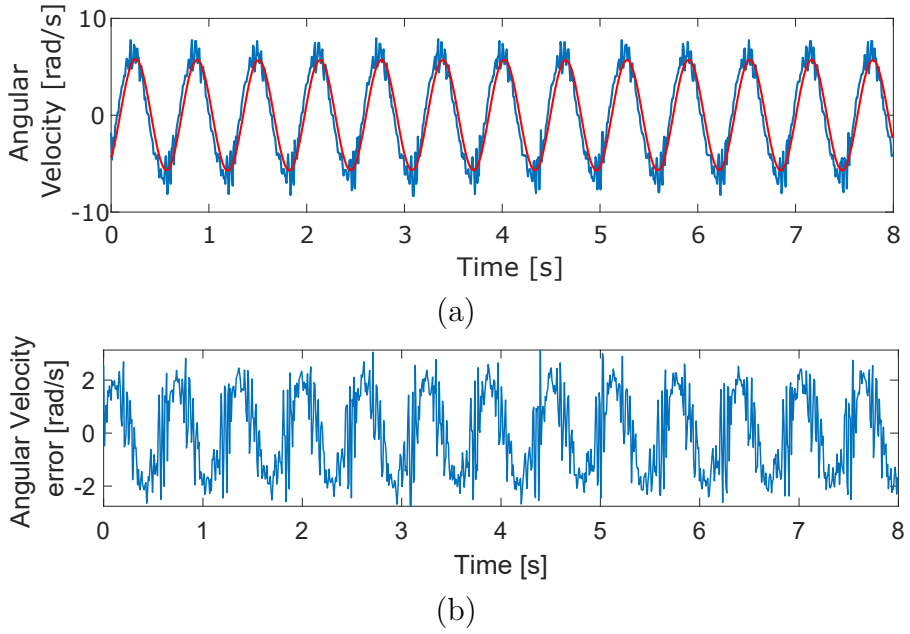

Figure 9.4: (a) Graphical Comparison and (b) Error plots between the measured and the Coulomb-Stribeck estimated velocity from the validation. The model estimations plotted in red and the experimental data in blue.

Part V

Final Remarks

10
Conclusions

The present work deals with modeling the nonlinearities of an eSEA actuator using different ML approaches, maintaining a compromise between complexity and accuracy while offering meaningful physical insights or interpretability into the system. Although the system has many nonlinearities, the contributions showed varied solutions to obtain accurate models.

In the first contribution, the focus of the identification tasks was to accurately model the elastic joint's characteristics. Therefore, the link was held in place, and experimental data about the joint's angular displacement was obtained. The proposed models were the ARMAX model, a linear model, a NARX-ANN representing the nonlinear model, and a hybrid model combining both previously mentioned algorithms. When comparing the three models, the hybrid model outperformed the other models by decreasing the MAE by 93% and 81.86% when compared to the ARMAX and NARX-ANN models, respectively. The coefficient of determination of the hybrid model was 0.99, which is as close to an ideal model as possible. These results show the potential of this methodology.

The second contribution is dedicated to studying friction models and evaluating the performance of PINNs for an identification task, for which multiple friction models found in the literature were chosen. In order to compare the performance of the PINNs, two models were selected to perform the black-box identification: the ARX and the ARMAX algorithms. The experimental data from the assembly was used with a swept sine excitation signal. All three models showed very promising results, with the ARMAX model outperforming the ARX model by decreasing the MAE error of 9.45%. The PINNs managed to perform the parameter identification task very accurately, extracting the maximum potential of each of the five models, considering their respective limitations. The best friction model was the LuGre model, which obtained a $R^2 = 0.942$. When compared to the best black-box models, the LuGre friction model outperformed the ARMAX model by decreasing the MAE by 30.83%. Furthermore, these results show the versatility and capacities of using physic-informed models, obtaining precise results while maintaining high interpretability.

The last contribution proposed a framework to identify the parameters of an ODE using video. Using pre-trained CNNs and transfer learning, the classification CNNs are repurposed to perform the state estimation of the

eSEA assembly using video. With the pose estimation complete, an LSTM layer is added to estimate the velocity and acceleration of the model. After obtaining the states, the gray-box identification is performed, estimating the friction parameters of two friction models. This framework was tested using the experimental data of the eSEA assembly. The results show that the transfer learning technique is highly accurate at estimating the states of the system from video. The friction models were obtained by adding a hardcoded layer representing the model and optimizing the parameters from the video. The framework results were adequate, obtaining precise state estimation and accurate identification of the friction models, with the Coulomb-Stribeck model obtaining a coefficient of determination of 0.89. This contribution showed the potential of this framework; considering its highly modular nature, the model can be improved by adding or changing parts of the estimation.

11
Future Works

In light of the results and discussion developed throughout this dissertation, future work can be suggested.

Regarding the application of hybrid models and PINNs in robotic systems, future work possibilities may include testing the approach using the same eSEA with a higher degree of freedom or applying it to other nonlinear systems such as a multi-arm pendulum on a cart [112], an EMPS system [113]. Furthermore, the model obtained could be applied and used as a base for a model-based controller. By combining novel ML algorithms such as transformers [114] or other novel ensemble approaches [115], one could test the effectiveness and the performance and compare it to this work result. Additionally, the approach's interpretability and generalization capacities could be improved using physics-based approaches such as Physics-Guided Neural Networks (PGNN) or PINNs [116–118].

Lastly, for the vision-based identification approach. The methodology's robustness could be improved by initially testing the method using other excitation signals and adding new degrees of freedom to the eSEA assembly. Following that, the methodology should be tested using videos of another nonlinear system, such as a multi-arm pendulum on a cart [112]. Given the modular aspect of the methodology, the estimation of the states could be improved by making it a single step and using ML algorithms such as 3D CNN [119], CNN-LSTM [120] or video transformers [121] in order to capture the video with the time element instead of the frames individually. Another step that might be improved is the identification, using algorithms such as PINNs or PGNNs. These could be easily implemented thanks to the module-based approach proposed in this work.

Bibliography

[1] JIANG, Y.; LI, X.; LUO, H.; YIN, S. ; KAYNAK, O.. **Quo vadis artificial intelligence?** Discover Artificial Intelligence, 2(1):4, 2022.

[2] MCCARTHY, J.. **What is artificial intelligence?** Technical report, Stanford University, Stanford, CA, USA, 2007.

[3] GENESERETH, M. R.; NILSSON, N. J.. **Logical foundations of artificial intelligence**. Morgan Kaufmann Publishers Inc., San Francisco, CA, USA, 1987.

[4] WU, Y.-C.; FENG, J.-W.. **Development and application of artificial neural network**. Wireless Personal Communications, 102:1645–1656, 2018.

[5] WANG, S.-C.; WANG, S.-C.. **Artificial neural network**. Interdisciplinary computing in java programming, p. 81–100, 2003.

[6] ZHANG, Z.; ZHANG, Z.. **Artificial neural network**. Multivariate time series analysis in climate and environmental research, p. 1–35, 2018.

[7] HAYKIN, S. O.. **Neural Networks and Learning Machines**. Pearson, Upper Saddle River, NJ, 3 edition, nov 2008.

[8] VRONTIS, D.; CHRISTOFI, M.; PEREIRA, V.; TARBA, S.; MAKRIDES, A. ; TRICHINA, E.. **Artificial intelligence, robotics, advanced technologies and human resource management: a systematic review**. Artificial intelligence and international HRM, p. 172–201, 2023.

[9] SHARMA, A.; PRASAD, K.; CHAKRASALI, S. V.; GOWDA V, D.; KUMAR, C.; CHATURVEDI, A. ; PAZHANI, A. A. J.. **Computer vision based healthcare system for identification of diabetes & its types using ai**. Measurement: Sensors, 27:100751, 2023.

[10] ALHARBI, F.; VAKANSKI, A.. **Machine learning methods for cancer classification using gene expression data: A review**. Bioengineering, 10(2):173, 2023.

[11] AN, Q.; RAHMAN, S.; ZHOU, J. ; KANG, J. J.. **A comprehensive review on machine learning in healthcare industry: classification, restrictions, opportunities and challenges**. Sensors, 23(9):4178, 2023.

[12] SURYADEVARA, C. K.. **Diabetes risk assessment using machine learning: A comparative study of classification algorithms**. IEJRD-International Multidisciplinary Journal, 8(4):10, 2023.

[13] OKOLI, U. I.; OBI, O. C.; ADEWUSI, A. O. ; ABRAHAMS, T. O.. **Machine learning in cybersecurity: A review of threat detection and defense mechanisms**. World Journal of Advanced Research and Reviews, 21(1):2286–2295, 2024.

[14] AHMAD, J.; ZIA, M. U.; NAQVI, I. H.; CHATTHA, J. N.; BUTT, F. A.; HUANG, T. ; XIANG, W.. **Machine learning and blockchain technologies for cybersecurity in connected vehicles**. Wiley Interdisciplinary Reviews: Data Mining and Knowledge Discovery, 14(1):e1515, 2024.

[15] BHARADIYA, J.. **Machine learning in cybersecurity: Techniques and challenges**. European Journal of Technology, 7(2):1–14, 2023.

[16] CHIUSO, A.; PILLONETTO, G.. **System identification: A machine learning perspective**. Annual Review of Control, Robotics, and Autonomous Systems, 2(1):281–304, 2019.

[17] PILLONETTO, G.; ARAVKIN, A.; GEDON, D.; LJUNG, L.; RIBEIRO, A. H. ; SCHÖN, T. B.. **Deep networks for system identification: A survey**. Automatica, 171:111907, 2025.

[18] SOORI, M.; AREZOO, B. ; DASTRES, R.. **Artificial intelligence, machine learning and deep learning in advanced robotics, a review**. Cognitive Robotics, 3:54–70, 2023.

[19] SOORI, M.; AREZOO, B. ; DASTRES, R.. **Artificial intelligence, machine learning and deep learning in advanced robotics, a review**. Cognitive Robotics, 3:54–70, 2023.

[20] SOORI, M.; AREZOO, B. ; DASTRES, R.. **Machine learning and artificial intelligence in cnc machine tools, a review**. Sustainable Manufacturing and Service Economics, 2:100009, 2023.

[21] WEISS, A.; WORTMEIER, A.-K. ; KUBICEK, B.. **Cobots in industry 4.0: A roadmap for future practice studies on human–robot collaboration**. IEEE Transactions on Human-Machine Systems, 51(4):335–345, 2021.

[22] KESHVARPARAST, A.; BATTINI, D.; BATTAIA, O. ; PIRAYESH, A.. **Collaborative robots in manufacturing and assembly systems:**

literature review and future research agenda. Journal of Intelligent Manufacturing, 35(5):2065–2118, 2024.

[23] LIU, L.; GUO, F.; ZOU, Z. ; DUFFY, V. G.. **Application, development and future opportunities of collaborative robots (cobots) in manufacturing: A literature review**. International Journal of Human–Computer Interaction, 40(4):915–932, 2024.

[24] HENTOUT, A.; AOUACHE, M.; MAOUDJ, A. ; AKLI, I.. **Human–robot interaction in industrial collaborative robotics: a literature review of the decade 2008–2017**. Advanced Robotics, 33(15-16):764–799, 2019.

[25] CHUTIMA, P.. **Assembly line balancing with cobots: An extensive review and critiques**. International Journal of Industrial Engineering Computations, 14(4):785–804, 2023.

[26] MAHALINGAM, D.; PATANKAR, A.; PHI, K.; CHAKRABORTY, N.; MCGANN, R. ; RAMAKRISHNAN, I.. **Containerized vertical farming using cobots**. In: 2024 IEEE INTERNATIONAL CONFERENCE ON ROBOTICS AND AUTOMATION (ICRA), p. 17897–17903, Yokohama, Japan, 2024. IEEE.

[27] JAVAID, M.; HALEEM, A.; SINGH, R. P.; RAB, S. ; SUMAN, R.. **Significant applications of cobots in the field of manufacturing**. Cognitive Robotics, 2:222–233, 2022.

[28] KIM, D.; KIM, S.-H.; KIM, T.; KANG, B. B.; LEE, M.; PARK, W.; KU, S.; KIM, D.; KWON, J.; LEE, H. ; OTHERS. **Review of machine learning methods in soft robotics**. Plos one, 16(2):e0246102, 2021.

[29] MAZUMDER, A.; SAHED, M.; TASNEEM, Z.; DAS, P.; BADAL, F.; ALI, M.; AHAMED, M.; ABHI, S.; SARKER, S.; DAS, S. ; OTHERS. **Towards next generation digital twin in robotics: Trends, scopes, challenges, and future**. Heliyon, 9(2), 2023.

[30] GLAESSGEN, E.; STARGEL, D.. **The digital twin paradigm for future nasa and us air force vehicles**. In: 53RD AIAA/ASME/ASCE/AHS/ASC STRUCTURES, STRUCTURAL DYNAMICS AND MATERIALS CONFERENCE 20TH AIAA/ASME/AHS ADAPTIVE STRUCTURES CONFERENCE 14TH AIAA, p. 1818, 2012.

[31] PHANDEN, R. K.; SHARMA, P. ; DUBEY, A.. **A review on simulation in digital twin for aerospace, manufacturing and robotics**. Materials Today: Proceedings, 38:174–178, 2021. 2nd International Conference on Future Learning Aspects of Mechanical Engineering.

[32] GRIEVES, M.; VICKERS, J.. **Digital Twin: Mitigating Unpredictable, Undesirable Emergent Behavior in Complex Systems**, p. 85–113. Springer International Publishing, Cham, 2017.

[33] PATTANAIK, R. K.; MOHANTY, M. N.. **Digital twin application on system identification and control**. Simulation Techniques of Digital Twin in Real-Time Applications: Design Modeling and Implementation, p. 123–162, 2024.

[34] SANFILIPPO, F.; ØKTER, M.; DALE, J.; TUAN, H. M. ; OTTESTAD, M.. **Revolutionising prosthetics and orthotics with affordable customisable open-source elastic actuators**. In: 2024 10TH INTERNATIONAL CONFERENCE ON AUTOMATION, ROBOTICS AND APPLICATIONS (ICARA), p. 57–63, Athens, Greece, 2024. IEEE.

[35] PRATT, G.; WILLIAMSON, M.. **Series elastic actuators**. Proceedings 1995 IEEE/RSJ International Conference on Intelligent Robots and Systems. Human Robot Interaction and Cooperative Robots, 1:399–406, 08 1995.

[36] TOUBAR, H.; AWAD, M. I.; BOUSHAKI, M. N.; NIU, Z.; KHALAF, K. ; HUSSAIN, I.. **Design, modeling, and control of a series elastic actuator with discretely adjustable stiffness (seadas)**. Mechatronics, 86:102863, 10 2022.

[37] MAJIDI, C.. **Soft robotics: A perspective—current trends and prospects for the future**. Soft Robotics, 1(1):5–11, 2014.

[38] VAN HAM, R.; SUGAR, T. G.; VANDERBORGHT, B.; HOLLANDER, K. W. ; LEFEBER, D.. **Compliant actuator designs**. IEEE Robotics & Automation Magazine, 16(3):81–94, 2009.

[39] DE SOUSA, D. H. B.; LOPES, F. R.; DO LAGO, A. W.; MEGGIOLARO, M. A. ; AYALA, H. V. H.. **Hybrid gray and black-box nonlinear system identification of an elastomer joint flexible robotic manipulator**. Mechanical Systems and Signal Processing, 200:110405, 2023.

[40] SARIYILDIZ, E.; CHEN, G. ; YU, H.. **A unified robust motion controller design for series elastic actuators**. IEEE/ASME Transactions on Mechatronics, 22(5):2229–2240, 2017.

[41] YOO, S.; CHUNG, W. K.. **Sea force/torque servo control with model-based robust motion control and link-side motion feedback**. In: 2015 IEEE INTERNATIONAL CONFERENCE ON ROBOTICS AND AUTOMATION (ICRA), p. 1042–1048, Seattle, WA, USA, 2015.

[42] DELLA SANTINA, C.; DURIEZ, C. ; RUS, D.. **Model-based control of soft robots: A survey of the state of the art and open challenges**. IEEE Control Systems Magazine, 43(3):30–65, 2023.

[43] GROTJAHN, M.; HEIMANN, B. ; ABDELLATIF, H.. **Identification of friction and rigid-body dynamics of parallel kinematic structures for model-based control**. Multibody System Dynamics, 11:273–294, 2004.

[44] QUARANTA, G.; LACARBONARA, W. ; MASRI, S. F.. **A review on computational intelligence for identification of nonlinear dynamical systems**. Nonlinear Dynamics, 99:1709–1761, 01 2020.

[45] ZHANG, L.; WEN, J.; LI, Y.; CHEN, J.; YE, Y.; FU, Y. ; LIVINGOOD, W.. **A review of machine learning in building load prediction**. Applied Energy, 285:116452, 2021.

[46] LJUNG, L.; ANDERSSON, C.; TIELS, K. ; SCHÖN, T. B.. **Deep learning and system identification**. IFAC-PapersOnLine, 53(2):1175–1181, 2020. 21st IFAC World Congress.

[47] NELLES, O.. **Nonlinear Dynamic System Identification**, p. 547–577. Springer Berlin Heidelberg, Berlin, Heidelberg, 2001.

[48] FERNANDES, D. L.; LOPES, F. R.; DO LAGO, A. W.; DE SOUSA, D. H. B.; MEGGIOLARO, M. A. ; AYALA, H. V. H.. **System identification of an elastomeric series elastic actuator using black-box models**. In: 2023 31ST MEDITERRANEAN CONFERENCE ON CONTROL AND AUTOMATION (MED), p. 569–574, Limassol, Cyprus, 2023. IEEE.

[49] JALALI, H.; DAMAVANDI, H.; KALHOR, A. ; MASOULEH, M. T.. **Experimental study on motion controller based on nn-arx and armax actuator identification for 3-dof delta parallel robot**. In: 2023 11TH RSI INTERNATIONAL CONFERENCE ON ROBOTICS AND

MECHATRONICS (ICROM), p. 782–787, Tehran, Islamic Republic of Iran, 2023. IEEE.

[50] WANG, C.; SHENG, B.; LI, Z.; SIVAN, M.; ZHANG, Z.-Q.; LI, G.-Q. ; XIE, S. Q.. **A lightweight series elastic actuator with variable stiffness: Design, modeling, and evaluation**. IEEE/ASME Transactions on Mechatronics, 28(6):3110–3119, 2023.

[51] RUDIN, C.. **Stop explaining black box machine learning models for high stakes decisions and use interpretable models instead**. Nature machine intelligence, 1(5):206–215, 2019.

[52] SIRCA, G.; ADELI, H.. **System identification in structural engineering**. Scientia Iranica, 19(6):1355–1364, 2012.

[53] EMAMINEJAD, N.; AKHAVIAN, R.. **Trustworthy ai and robotics: Implications for the aec industry**. Automation in Construction, 139:104298, 2022.

[54] NASER, M.. **An engineer's guide to explainable artificial intelligence and interpretable machine learning: Navigating causality, forced goodness, and the false perception of inference**. Automation in Construction, 129:103821, 2021.

[55] PINTELAS, E.; LIVIERIS, I. E. ; PINTELAS, P.. **A grey-box ensemble model exploiting black-box accuracy and white-box intrinsic interpretability**. Algorithms, 13(1), 2020.

[56] RAISSI, M.; PERDIKARIS, P. ; KARNIADAKIS, G.. **Physics-informed neural networks: A deep learning framework for solving forward and inverse problems involving nonlinear partial differential equations**. Journal of Computational Physics, 378:686–707, 2019.

[57] NASIRI, P.; DARGAZANY, R.. **Reduced-pinn: An integration-based physics-informed neural networks for stiff odes**. arXiv preprint arXiv:2208.12045, 2022.

[58] BATY, H.. **Solving stiff ordinary differential equations using physics informed neural networks (pinns): simple recipes to improve training of vanilla-pinns**. arXiv preprint arXiv:2304.08289, 2023.

[59] DANEKER, M.; ZHANG, Z.; KARNIADAKIS, G. E. ; LU, L.. **Systems biology: Identifiability analysis and parameter identification via**

systems-biology-informed neural networks. In: COMPUTATIONAL MODELING OF SIGNALING NETWORKS, p. 87–105. Springer, 2023.

[60] DENG, J.; DONG, W.; SOCHER, R.; LI, L.-J.; LI, K. ; FEI-FEI, L.. **Imagenet: A large-scale hierarchical image database**. In: 2009 IEEE CONFERENCE ON COMPUTER VISION AND PATTERN RECOGNITION, p. 248–255, Miami, FL, 2009. Ieee.

[61] MEENA, G.; MOHBEY, K. K.; INDIAN, A. ; KUMAR, S.. **Sentiment analysis from images using vgg19 based transfer learning approach**. Procedia Computer Science, 204:411–418, 2022. International Conference on Industry Sciences and Computer Science Innovation.

[62] ISLAM, S.; ELMEKKI, H.; ELSEBAI, A.; BENTAHAR, J.; DRAWEL, N.; RJOUB, G. ; PEDRYCZ, W.. **A comprehensive survey on applications of transformers for deep learning tasks**. Expert Systems with Applications, p. 122666, 2023.

[63] BEINTEMA, G. I.; TOTH, R. ; SCHOUKENS, M.. **Non-linear state-space model identification from video data using deep encoders**. IFAC-PapersOnLine, 54(7):697–701, 2021. 19th IFAC Symposium on System Identification SYSID 2021.

[64] JAQUES, M.; ASENOV, M.; BURKE, M. ; HOSPEDALES, T. M.. **Vision-based system identification and 3d keypoint discovery using dynamics constraints**. CoRR, abs/2109.05928, 2021.

[65] AL-SHANOON, A.; LANG, H.. **Robotic manipulation based on 3-d visual servoing and deep neural networks**. Robotics and Autonomous Systems, 152:104041, 2022.

[66] LU, J.; LIU, F.; GIRERD, C. ; YIP, M. C.. **Image-based pose estimation and shape reconstruction for robot manipulators and soft, continuum robots via differentiable rendering**. In: 2023 IEEE INTERNATIONAL CONFERENCE ON ROBOTICS AND AUTOMATION (ICRA), p. 560–567, London, UK, 2023.

[67] BALANJI, H. M.; TURGUT, A. E. ; TUNC, L. T.. **A novel vision-based calibration framework for industrial robotic manipulators**. Robotics and Computer-Integrated Manufacturing, 73:102248, 2022.

[68] HEIDEN, E.; LIU, Z.; VINEET, V.; COUMANS, E. ; SUKHATME, G. S.. **Inferring articulated rigid body dynamics from rgbd video**.

In: 2022 IEEE/RSJ INTERNATIONAL CONFERENCE ON INTELLIGENT ROBOTS AND SYSTEMS (IROS), p. 8383–8390, Kyoto, Japan, 2022.

[69] ASENOV, M.; BURKE, M.; ANGELOV, D.; DAVCHEV, T.; SUBR, K. ; RAMAMOORTHY, S.. **Vid2param: Modeling of dynamics parameters from video**. IEEE Robotics and Automation Letters, 5(2):414–421, 2020.

[70] HOFHERR, F.; KOESTLER, L.; BERNARD, F. ; CREMERS, D.. **Neural implicit representations for physical parameter inference from a single video**. In: IEEE/CVF WINTER CONFERENCE ON APPLICATIONS OF COMPUTER VISION, Waikoloa, Hawaii, 2023.

[71] LOPES, F. R.; MEGGIOLARO, M. A.. **Design of a low-cost series elastic actuator for application in robotic manipulators**. Proceedings of the 26th International Congress of Mechanical Engineering, 2021.

[72] NATKE, H.. **Recent trends in system identification**. In: STRUCTURAL DYNAMICS-VOL 1, p. 283–289. Routledge, 2022.

[73] BILLINGS, S. A.. **Nonlinear system identification: NARMAX methods in the time, frequency, and spatio-temporal domains**. John Wiley & Sons, Nashville, TN, sep 2013.

[74] SJÖBERG, J.; ZHANG, Q.; LJUNG, L.; BENVENISTE, A.; DELYON, B. ; ET AL.. **Nonlinear black-box modeling in system identification: a unified overview**. Automatica, 31:1691–1724, 12 1995.

[75] SIEGELMANN, H. T.; HORNE, B. G. ; GILES, C. L.. **Computational capabilities of recurrent narx neural networks**. IEEE Transactions on Systems, Man, and Cybernetics, Part B (Cybernetics), 27(2):208–215, 1997.

[76] LU, L.; MENG, X.; MAO, Z. ; KARNIADAKIS, G. E.. **Deepxde: A deep learning library for solving differential equations**. SIAM review, 63(1):208–228, 2021.

[77] WANG, S.; SANKARAN, S.; WANG, H. ; PERDIKARIS, P.. **An expert's guide to training physics-informed neural networks**. arXiv preprint arXiv:2308.08468, 2023.

[78] ZENG, C.; BURGHARDT, T. ; GAMBARUTO, A. M.. **Training dynamics in physics-informed neural networks with feature mapping**. arXiv preprint arXiv:2402.06955, 2024.

[79] KEESMAN, K. J.. **System identification: an introduction**. Advanced Textbooks in Control and Signal Processing. Springer, Guildford, England, 2011 edition, may 2011.

[80] OLSEN, S. G.; BONE, G. M.. **Modelling of robotic bulldozing operations for autonomous control**. In: 2011 24TH CANADIAN CONFERENCE ON ELECTRICAL AND COMPUTER ENGINEERING(CCECE), p. 001188–001193, Niagara Falls, ON, Canada, 2011.

[81] LAGO, A. W. C.; CAMERINI, I. G.; SOUSA, L. C.; DE SOUSA, D. H. B.; LOPES, F. R.; MEGGIOLARO, M. A. ; AYALA, H. V. H.. **Black-box identification with static neural networks of nonlinearities of an elastomer-based elastic joint manipulator**. In: 2023 INTERNATIONAL JOINT CONFERENCE ON NEURAL NETWORKS (IJCNN), p. 1–7, Queensland, Australia, 2023. IEEE.

[82] SAK, H.; SENIOR, A. ; BEAUFAYS, F.. **Long short-term memory based recurrent neural network architectures for large vocabulary speech recognition**, 2014.

[83] ASLAN, S.; ÖZALP, R.; UÇAR, A. ; GÜZELIŞ, C.. **New cnn and hybrid cnn-lstm models for learning object manipulation of humanoid robots from demonstration**. Cluster Computing, 25, 06 2022.

[84] STAUDEMEYER, R. C.; MORRIS, E. R.. **Understanding lstm – a tutorial into long short-term memory recurrent neural networks**, 2019.

[85] LECUN, Y.; BENGIO, Y. ; HINTON, G.. **Deep learning**. nature, 521(7553):436–444, 2015.

[86] GOODFELLOW, I.; BENGIO, Y. ; COURVILLE, A.. **Deep Learning**. Adaptive Computation and Machine Learning series. MIT Press, London, England, 2016.

[87] PAN, S. J.; YANG, Q.. **A survey on transfer learning**. IEEE Transactions on Knowledge and Data Engineering, 22(10):1345–1359, 2010.

[88] MEENA, G.; MOHBEY, K. K.; INDIAN, A. ; KUMAR, S.. **Sentiment analysis from images using vgg19 based transfer learning approach**. Procedia Computer Science, 204:411–418, 2022.

[89] POPOVA, E.; POPOV, V. L.. **The research works of coulomb and amontons and generalized laws of friction**. Friction, 3:183–190, 2015.

[90] MARQUES, F.; FLORES, P.; PIMENTA CLARO, J. ; LANKARANI, H. M.. **A survey and comparison of several friction force models for dynamic analysis of multibody mechanical systems**. Nonlinear Dynamics, 86:1407–1443, 2016.

[91] OLSSON, H.; ÅSTRÖM, K.; CANUDAS DE WIT, C.; GÄFVERT, M. ; LISCHINSKY, P.. **Friction models and friction compensation**. European Journal of Control, 4(3), 1998.

[92] DE COULOMB, C. A.. **Théorie des machines simples: en ayant égard au frottement de leurs parties et à la roideur des cordages, par C.-A. Coulomb... Nouvelle édition...** Bachelier, Paris, France, 1821.

[93] STRIBECK, R.. **Die wesentlichen eigenschaften der gleit-und rollenlager**. Zeitschrift des Vereines Deutscher Ingenieure, 46:1341–1348, 1902.

[94] JOHANASTROM, K.; CANUDAS-DE-WIT, C.. **Revisiting the lugre friction model**. IEEE Control systems magazine, 28(6):101–114, 2008.

[95] DAHL, P. R.. **A solid friction model**. Technical Report TOR-0158(3107–18)-1, 1968.

[96] CHOU, D.. **Dahl friction modeling**. PhD thesis, Massachusetts Institute of Technology, 2004.

[97] DE WIT, C. C.; OLSSON, H.; ASTROM, K. ; LISCHINSKY, P.. **Dynamic friction models and control design**. In: 1993 AMERICAN CONTROL CONFERENCE, p. 1920–1926, San Francisco, CA, USA, 1993. IEEE.

[98] DE WIT, C. C.; OLSSON, H.; ASTROM, K. J. ; LISCHINSKY, P.. **A new model for control of systems with friction**. IEEE Transactions on automatic control, 40(3):419–425, 1995.

[99] PIATKOWSKI, T.. **Dahl and lugre dynamic friction models—the analysis of selected properties**. Mechanism and Machine Theory, 73:91–100, 2014.

[100] JIN, M.; LEE, J. ; TSAGARAKIS, N. G.. **Model-free robust adaptive control of humanoid robots with flexible joints**. IEEE Transactions on Industrial Electronics, 64(2):1706–1715, 2017.

[101] MADSEN, E.; ROSENLUND, O. S.; BRANDT, D. ; ZHANG, X.. **Comprehensive modeling and identification of nonlinear joint dynamics for collaborative industrial robot manipulators**. Control Engineering Practice, 101:104462, 2020.

[102] CHIARADIA, D.; TISENI, L. ; FRISOLI, A.. **Compact series viscoelastic joint (svej) for smooth torque control**. IEEE Transactions on Haptics, 13:226–232, 01 2020.

[103] HAN, S.; WANG, H.; TIAN, Y. ; YU, H.. **Enhanced extended state observer-based model-free force control for a series elastic actuator**. Mechanical Systems and Signal Processing, 183:109584, 01 2023.

[104] SWEVERS, J.; VERDONCK, W. ; DE SCHUTTER, J.. **Dynamic model identification for industrial robots**. IEEE Control Systems, 27:58–71, 10 2007.

[105] AYALA, H. V. H.; GRITTI, M. C. ; DOS SANTOS COELHO, L.. **An r library for nonlinear black-box system identification**. SoftwareX, 11:100495, 2020.

[106] MADSEN, E.; ROSENLUND, O. S.; BRANDT, D. ; ZHANG, X.. **Comprehensive modeling and identification of nonlinear joint dynamics for collaborative industrial robot manipulators**. Control Engineering Practice, 101, 2020.

[107] KERMANI, M. R.; PATEL, R. V. ; MOALLEM, M.. **Friction identification and compensation in robotic manipulators**. IEEE Transactions on Instrumentation and Measurement, 56(6):2346–2353, 2007.

[108] BONA, B.; INDRI, M.. **Friction compensation in robotics: an overview**. In: PROCEEDINGS OF THE 44TH IEEE CONFERENCE ON DECISION AND CONTROL, p. 4360–4367, Seville, Spain, 2005.

[109] JUNIOR, J.; BALTHAZAR, J.; RIBEIRO, M.; JANZEN, F. ; TUSSET, A.. **Dynamic model of a robotic manipulator with one degree of freedom with friction component**. International Journal of Robotics and Control Systems, 05 2023.

[110] M. AHMADIZADEH, A. M. S.; FOOLADI, M.. **Dynamic modeling of closed-chain robotic manipulators in the presence of frictional dynamic forces: A planar case**. Mechanics Based Design of Structures and Machines, 51(8):4347–4367, 2023.

[111] LI, X.; GU, J.; SUN, X.; LI, J. ; TANG, S.. **Parameter identification of robot manipulators with unknown payloads using an improved chaotic sparrow search algorithm**. Applied Intelligence, 52:1–11, 07 2022.

[112] KAHEMAN, K.; FASEL, U.; BRAMBURGER, J. J.; STROM, B.; KUTZ, J. N. ; BRUNTON, S. L.. **The experimental multi-arm pendulum on a cart: A benchmark system for chaos, learning, and control**. HardwareX, 15:e00465, 2023.

[113] JANOT, A.; GAUTIER, M. ; BRUNOT, M.. **Data set and reference models of emps**. In: NONLINEAR SYSTEM IDENTIFICATION BENCHMARKS, 2019.

[114] GENEVA, N.; ZABARAS, N.. **Transformers for modeling physical systems**. CoRR, abs/2010.03957, 2020.

[115] NEGRINI, E.; CITTI, G. ; CAPOGNA, L.. **A neural network ensemble approach to system identification**. CoRR, abs/2110.08382, 2021.

[116] GÖTTE, R.-S.; TIMMERMANN, J.. **Composed physics-and data-driven system identification for non-autonomous systems in control engineering**. In: 2022 3RD INTERNATIONAL CONFERENCE ON ARTIFICIAL INTELLIGENCE, ROBOTICS AND CONTROL (AIRC), p. 67–76, Cairo, Egypt, 2022. IEEE.

[117] LIU, X.; CHEN, D.; WEI, W.; ZHU, X. ; YU, W.. **Interpretable sparse system identification: Beyond recent deep learning techniques on time-series prediction**. In: THE TWELFTH INTERNATIONAL CONFERENCE ON LEARNING REPRESENTATIONS, Vienna, Austria, 2024.

[118] LIU, Y.; WANG, L. ; NG, B. F.. **A hybrid model-data-driven framework for inverse load identification of interval structures based on physics-informed neural network and improved kalman filter algorithm**. Applied Energy, 359:122740, 2024.

[119] WANG, C.. **A review on 3d convolutional neural network**. In: 2023 IEEE 3RD INTERNATIONAL CONFERENCE ON POWER, ELECTRONICS AND COMPUTER APPLICATIONS (ICPECA), p. 1204–1208, Shenyang, China, 2023.

[120] YANG, R.; SINGH, S. K.; TAVAKKOLI, M.; AMIRI, N.; YANG, Y.; KARAMI, M. A. ; RAI, R.. **Cnn-lstm deep learning architecture for computer**

vision-based modal frequency detection. Mechanical Systems and Signal Processing, 144:106885, 2020.

[121] SELVA, J.; JOHANSEN, A. S.; ESCALERA, S.; NASROLLAHI, K.; MOESLUND, T. B. ; CLAPES, A.. **Video transformers: A survey**. IEEE Transactions on Pattern Analysis amp; Machine Intelligence, 45(11):12922–12943, 2023.